Please cite this article in press as: Cebrián-Silla et al., Unique Organization of the Nuclear Envelope in the Post-natal Quiescent Neural Stem Cells, Stem Cell Reports (2017), http://dx.doi.org/10.1016/j.stemcr.2017.05.024

Stem Cell Reports
Article

ISSCR

OPEN ACCESS

Unique Organization of the Nuclear Envelope in the Post-natal Quiescent Neural Stem Cells

Arantxa Cebrián-Silla,[1] Clara Alfaro-Cervelló,[2] Vicente Herranz-Pérez,[1,3] Naoko Kaneko,[4] Dae Hwi Park,[5] Kazunobu Sawamoto,[4,6] Arturo Alvarez-Buylla,[5] Daniel A. Lim,[5,7] and José Manuel García-Verdugo[1,8,*]

[1]Laboratory of Comparative Neurobiology, Institute Cavanilles, University of Valencia, CIBERNED, 46980 Valencia, Spain
[2]Servicio de Anatomía Patológica, Hospital Clínico Universitario de Valencia, 46010 Valencia, Spain
[3]Predepartamental Unit of Medicine, Faculty of Health Sciences, Universitat Jaume I, 12071 Castelló de la Plana, Spain
[4]Department of Developmental and Regenerative Biology, Nagoya City University Graduate School of Medical Sciences, Nagoya 467-8601, Japan
[5]Department of Neurological Surgery, The Eli and Edythe Broad Center of Regeneration Medicine, Stem Cell Research, University of California, San Francisco, San Francisco, CA 94143, USA
[6]Division of Neural Development and Regeneration, National Institute for Physiological Sciences, Okazaki, Aichi 444-8585, Japan
[7]Veterans Affairs Medical Center, University of California, San Francisco, San Francisco, CA 94143, USA
[8]Multiple Sclerosis and Neuroregeneration Mixed Unit, IIS Hospital La Fe, 46026 Valencia, Spain
*Correspondence: j.manuel.garcia@uv.es
http://dx.doi.org/10.1016/j.stemcr.2017.05.024

SUMMARY

Neural stem cells (B1 astrocytes; NSCs) in the adult ventricular-subventricular-zone (V-SVZ) originate in the embryo. Surprisingly, recent work has shown that B1 cells remain largely quiescent. They are reactivated postnatally to function as primary progenitors for neurons destined for the olfactory bulb and some corpus callosum oligodendrocytes. The cellular and molecular properties of quiescent B1 cells remain unknown. Here we found that a subpopulation of B1 cells has a unique nuclear envelope invagination specialization similar to envelope-limited chromatin sheets (ELCS), reported in certain lymphocytes and some cancer cells. Using molecular markers, [^{3}H]thymidine birth-dating, and Ara-C, we found that B1 cells with ELCS correspond to quiescent NSCs. ELCS begin forming in embryonic radial glia cells and represent a specific nuclear compartment containing particular epigenetic modifications and telomeres. These results reveal a unique nuclear compartment in quiescent NSCs, which is useful for identifying these primary progenitors and study their gene regulation.

INTRODUCTION

Neural stem cells (NSCs) persist in the ventricular-subventricular zone (V-SVZ) in the walls of the lateral ventricles of many adult mammals. This neurogenic niche is composed of NSCs (B1 astrocytes) that divide slowly to give rise to transit-amplifying cells (C cells), which in turn generate neuroblasts (A cells) that migrate tangentially to the olfactory bulb (Alvarez-Buylla et al., 2001; Lois and Alvarez-Buylla, 1994). B1 cells are characterized by their highly polarized morphology, which presents a thin apical process that contacts the lateral ventricle (LV) and cerebrospinal fluid (CSF). Moreover, they also exhibit a basal process ending on blood vessels (Doetsch et al., 2002; Mirzadeh et al., 2008; Tavazoie et al., 2008). The apical surface of B1 cells is surrounded by large apical surfaces of ependymal cells in a pinwheel configuration (Mirzadeh et al., 2008). NSCs cells can exist as quiescent/slowly dividing (qNSCs) or activated/dividing (aNSCs) primary progenitors. It has been suggested that these two populations represent two functionally distinct types of NSCs which differ in their cell-cycle status and molecular properties (Codega et al., 2014; Llorens-Bobadilla et al., 2015; Mich et al., 2014; Morshead et al., 1994). aNSCs maintain the expression of glial fibrillary acidic protein (GFAP), CD133, epidermal growth factor receptor (EGFR), and Nestin, while qNSCs preserve the expression of GFAP, CD133, but not EGFR and Nestin. Furthermore, qNSCs do not express proliferation markers and survive infusion of cytosine-β-D-arabinofuranoside (Ara-C), which eliminates the aNSC population (Codega et al., 2014; Doetsch et al., 1999; Morshead et al., 1994; Pastrana et al., 2009). Recently, it has been suggested that qNSCs have an embryonic origin; pre-B1 cells are produced during mid-fetal development (embryonic day 13.5 [E13.5] to E15.5), remaining relatively quiescent until reactivated postnatally (Fuentealba et al., 2015; Furutachi et al., 2015).

The maintenance of quiescence is thought to be directly co-related with the regulation of gene expression, which can be observed as large heterochromatic regions likely corresponding to silenced genes (Capelson and Corces, 2012). Previously, it has been suggested that a distinctive nuclear morphology is linked to the maintenance of pluripotency (Gorkin et al., 2014; Ito et al., 2014; Sexton and Cavalli, 2013), and possibly associated with quiescence. However, despite NSC chromatin presenting peculiar topographical configurations (Krijger et al., 2016; Peric-Hupkes et al., 2010; Phillips-Cremins et al., 2013), the relationship between chromatin organization and nuclear morphology remains poorly understood. Previous studies have shown that murine and human fetal V-SVZ B cells have irregular nuclei that exhibit unusual nuclear envelope (NE)

Please cite this article in press as: Cebrián-Silla et al., Unique Organization of the Nuclear Envelope in the Post-natal Quiescent Neural Stem Cells, Stem Cell Reports (2017), http://dx.doi.org/10.1016/j.stemcr.2017.05.024

invaginations (Capilla-Gonzalez et al., 2014; Doetsch et al., 1997; Guerrero-Cazares et al., 2011).

Here we have studied the fine ultrastructure and three-dimensional (3D) organization of these invaginations and show that they correspond to envelope-limited chromatin sheets (ELCS). These structures were originally described by Davies and Small (1968) in neutrophils, and named envelope-limited sheets (ELS). ELS have an unusual type of nuclear morphology characterized by the presence of a sheet of chromatin (~30 nm thick) bound on two sides by the inner nuclear membrane (INM), creating a highly reproducible and regular "sandwich" of 40 nm thickness (Davies and Small, 1968). These structures, later called ELCS, are associated with the NE proteins Lamin B, Lamin B receptor (LBR), and Lap2 (Ghadially, 1997; Olins et al., 1998; Olins and Olins, 2009). Interestingly, ELCS have only been reported in certain lymphocytes and some cancer cells, including the CNS neuroectodermal tumor medulloblastoma (Tani et al., 1971). Furthermore, we show here that V-SVZ B1 cells with ELCS correspond to qNSCs in mice.

RESULTS

A Subset of B Cells Has Nuclear Envelope-Limited Chromatin Sheets

Unlike other V-SVZ cell types, B cells in the V-SVZ present an irregular nucleus and, occasionally, NE invaginations (Capilla-Gonzalez et al., 2014; Doetsch et al., 1997; Guerrero-Cazares et al., 2011). These nuclear structures show a single sheet of chromatin bound on two sides by the INM and outer nuclear membrane (ONM), resembling the nuclear ELCS previously described in neutrophils (Olins and Olins, 2009). However, whether these nuclear ELCS are present in all B cells or in a distinct subpopulation has not been studied. To improve the characterization of B cells containing ELCS, we examined the V-SVZ of P60 mice by transmission electron microscopy (TEM). We found that in single TEM ultrathin sections, ELCS were frequently present in B cells (11.9% ± 0.4%; 1,052 B cells including B1 and B2 cells, defined as cells with or without apical ending, respectively; n = 4) (Figures 1A and 1B). To better estimate the proportion of B cells with ELCS, we used serial section 3D reconstruction of the entire nuclei. Almost half of the analyzed B cells (46% ± 3%; 160 B cells, n = 4) presented ELCS. These astrocytes were found forming groups of two to four cells in the whole length of the lateral walls of the LVs, but not in the adjacent striatum (0/102; n = 3). We did not find differences in the percentage of B cells with ELCS among different rostrocaudal levels (anterior 12.67%, medial 11.00%, posterior 10.34%; $p > 0.05$, not significant; bregma 1.18–0.02). In serial reconstructions, no ependymal, C cells, or A cells exhibited this type of NE (83, 20, and 140 studied cells at post-natal day 60 [P60]; n = 4) (Figures S1A–S1D). In addition, B cells with ELCS displayed one or two nuclear ELCS with a length of 0.4–2 μm (studied in 50 cells; n = 3) encompassing ~0.20% of the total nuclear volume (for image sequence reconstruction, see Movie S1). The ELCS ONM showed ribosomes attached to it and did not contain nuclear pores. Heterochromatin clumps were usually associated to nuclear ELCS endpoints (Figures 1C and 1D). Interestingly, 90.1% ± 0.1% of ELCS (80 B cells, n = 4) were internalized within the irregular nucleus (Figures 1E and 1F).

To better characterize ELCS in B cells, we performed pre-embedding immunogold stainings and independently examined the expression of brain lipid-binding protein (BLBP), GFAP, Nestin, EGFR, and Glast, which differentially marked B cells. We found out that ELCS were present in $GFAP^+$, $BLBP^+$, and $Glast^+$ B cells (Figures 1G–1M). The majority of cells with ELCS showed no expression of EGFR (1/20) and none were positive for Nestin. This expression profile overlaps with that recently described for qNSCs (Codega et al., 2014).

B1 cells (contacting the CSF in the pinwheel center) are a relatively quiescent or slow-diving NSCs derived from radial glia (Fuentealba et al., 2015; Kriegstein and Alvarez-Buylla, 2009). To determine whether B1 cells with identified apical ending present nuclear ELCS, we performed serial section reconstructions using confocal microscopy of the ventricular wall whole-mount preparation (Mirzadeh et al., 2010). In serial confocal microscopy sections of V-SVZ whole mounts, the apical terminations of $GFAP^+$ B1 cells were localized in the pinwheel center and tracked up to cell nuclei delimited by Lamin B and DAPI. The majority (83% ± 1%; 104 pinwheels; n = 13) of B1 cells with apical endings on pinwheels had irregular NE and bright Lamin B labeling (Figures 2A–2H). Analyzing serial whole-mount ultrathin sections by TEM (20 cells; n = 2), we confirmed that the deep nuclear invaginations of B1 cells corresponded to the ELCS zone (Figures 2J–2L). Hence, we conclude that a subpopulation of B1 cells contains ELCS.

Interestingly, single TEM sections revealed that ELCS were also present in a small subset of subgranular zone astrocytes (1.5% ± 0.6%; P60; 268 cells; n = 3), identified as the hippocampal dentate gyrus NSCs (Klempin and Kempermann, 2007; Seri et al., 2004). To confirm that this small fraction of astrocytes corresponded to radial astrocytes, we performed post-embedding GFAP and BLBP immunostainings in semithin sections (Figure S2). We found that Glast or BLBP cells with radial morphology exhibited ELCS in their nuclei. These results suggest that a subpopulation of NSCs present a unique NE.

ELCS in a Subset of Dormant B Cells

EGFR expression has been associated with the activation of B1 cells. We found out that 13.3% ± 0.6% of B1 cells were

Please cite this article in press as: Cebrián-Silla et al., Unique Organization of the Nuclear Envelope in the Post-natal Quiescent Neural Stem Cells, Stem Cell Reports (2017), http://dx.doi.org/10.1016/j.stemcr.2017.05.024

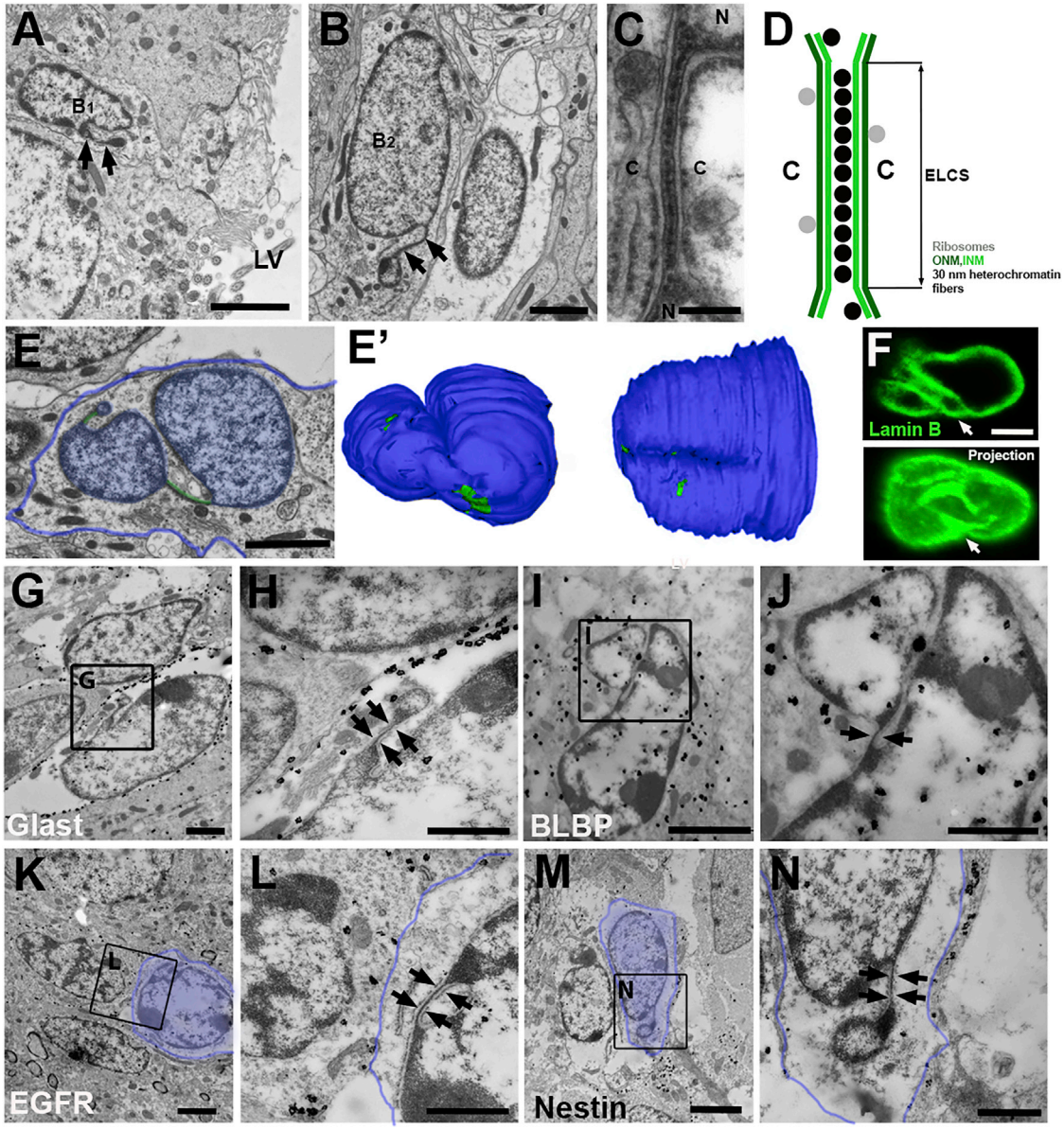

Figure 1. V-SVZ B Cells Show Nuclear Envelope-Limited Chromatin Sheets

(A and B) TEM images of B1 cell contacting the LV and B2 cell, showing nuclear ELCS (arrows).

(C and D) Nuclear ELCS TEM micrograph and its schematic diagram showing the typical configuration of 30-nm heterochromatin fibers bound on two sides by the INM and ONM. See also Movie S1. C, cytoplasm; N, nucleus.

(E) TEM pseudo-colored image of B cell with ELCS showing the plasmatic membrane and nucleus in blue, and ELCS in green. (E') 3D nuclear reconstruction of B cell in (E). Note that nuclear ELCS are represented in green.

(F) V-SVZ B cell nucleus labeled with Lamin B (green) showing an irregular morphology with ELCS (arrow). The 3D nuclear projection shows that ELCS (arrow) are internalized within the nucleus.

(G–J) Immunogold stainings for Glast (G, H) and BLBP (I, J) markers showing that B cells with ELCS (arrows) express Glast$^+$ and BLBP$^+$.

(K–N) Immunogold stainings for EGFR and Nestin markers showing that B cells with ELCS (pseudo-colored in blue, arrows) are negative for these markers (note the internal positive control in adjacent cells).

Scale bar, 2 μm (A, B, E, F, H, J, L, N), 1 μm (G, I, K, M), and 200 nm (C).

Please cite this article in press as: Cebrián-Silla et al., Unique Organization of the Nuclear Envelope in the Post-natal Quiescent Neural Stem Cells, Stem Cell Reports (2017), http://dx.doi.org/10.1016/j.stemcr.2017.05.024

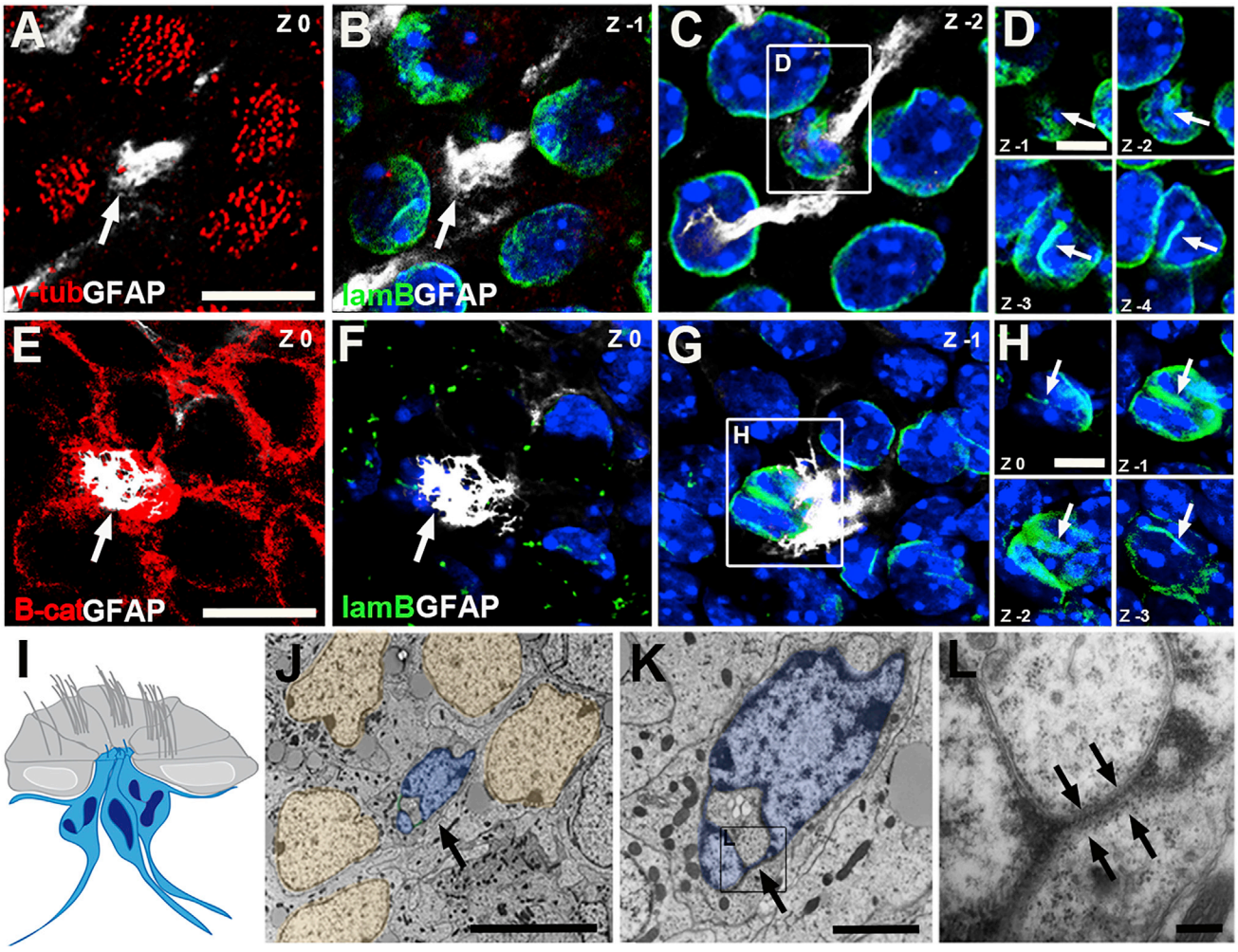

Figure 2. B1 Cells within Pinwheels Show Nuclear ELCS

(A–H) Confocal images of a V-SVZ whole mount immunostained for γ-tubulin (A–D, red), β-catenin (E–H, red), GFAP (white), and Lamin B (green) to visualize the nucleus of uniciliated B1 cells. Insets (D and H) show sequential z slices of the very irregular nucleus and high expression of Lamin B in B1 cells (white arrows).

(I) Schematic showing that two types of B1 cells (blue) can be distinguished depending on their nuclear morphology.

(J) Pseudo-colored TEM image of a whole mount showing the nuclei of ependymal cells in brown and B1 cell nucleus with ELCS in the center of the pinwheel (blue, arrow).

(K and L) Higher-magnification micrographs of the type B1 cell with ELCS (arrows) in (J).

Scale bars, 15 μm (A, E), 10 μm (J), 5 μm (D, H), 2 μm (K), and 200 nm (L).

$EGFR^+$ (30 pinwheels; n = 4) and did not display ELCS, while Lamin B expression was weak (9/30) or absent (21/30) (Figures 3A and 3B). Therefore, we hypothesized that ELCS could be associated with quiescent B1 cells. To test this hypothesis, we injected a group of P60 mice (n = 3) with [^{3}H]thymidine (^{3}H-Thy) (four injections, every 2 hr) and euthanized them 2 hr after the last injection, to label the proliferating cells (Figure 3C). ^{3}H-Thy-labeled cells were mapped in serial 1.5-μm semithin sections sampled at different rostrocaudal levels in the V-SVZ. One hundred and eighty ^{3}H-Thy-labeled cells were then resectioned for serial TEM analysis. Thirty corresponded to B cells, displaying irregular contours, light cytoplasm, and intermediate filaments. None of these 30 B cells had a nuclear ELCS (Figures 3D–3F), suggesting that actively dividing B cells do not contain ELCS.

We next examined whether B cells that have undergone cell division can develop nuclear ELCS 2 months later. Mice (n = 3) were injected with ^{3}H-Thy (as mentioned above) and label-retaining cells (LRCs) were studied 2 months later under TEM (Figure 3C′). ^{3}H-Thy-LRCs at this time were very

Please cite this article in press as: Cebrián-Silla et al., Unique Organization of the Nuclear Envelope in the Post-natal Quiescent Neural Stem Cells, Stem Cell Reports (2017), http://dx.doi.org/10.1016/j.stemcr.2017.05.024

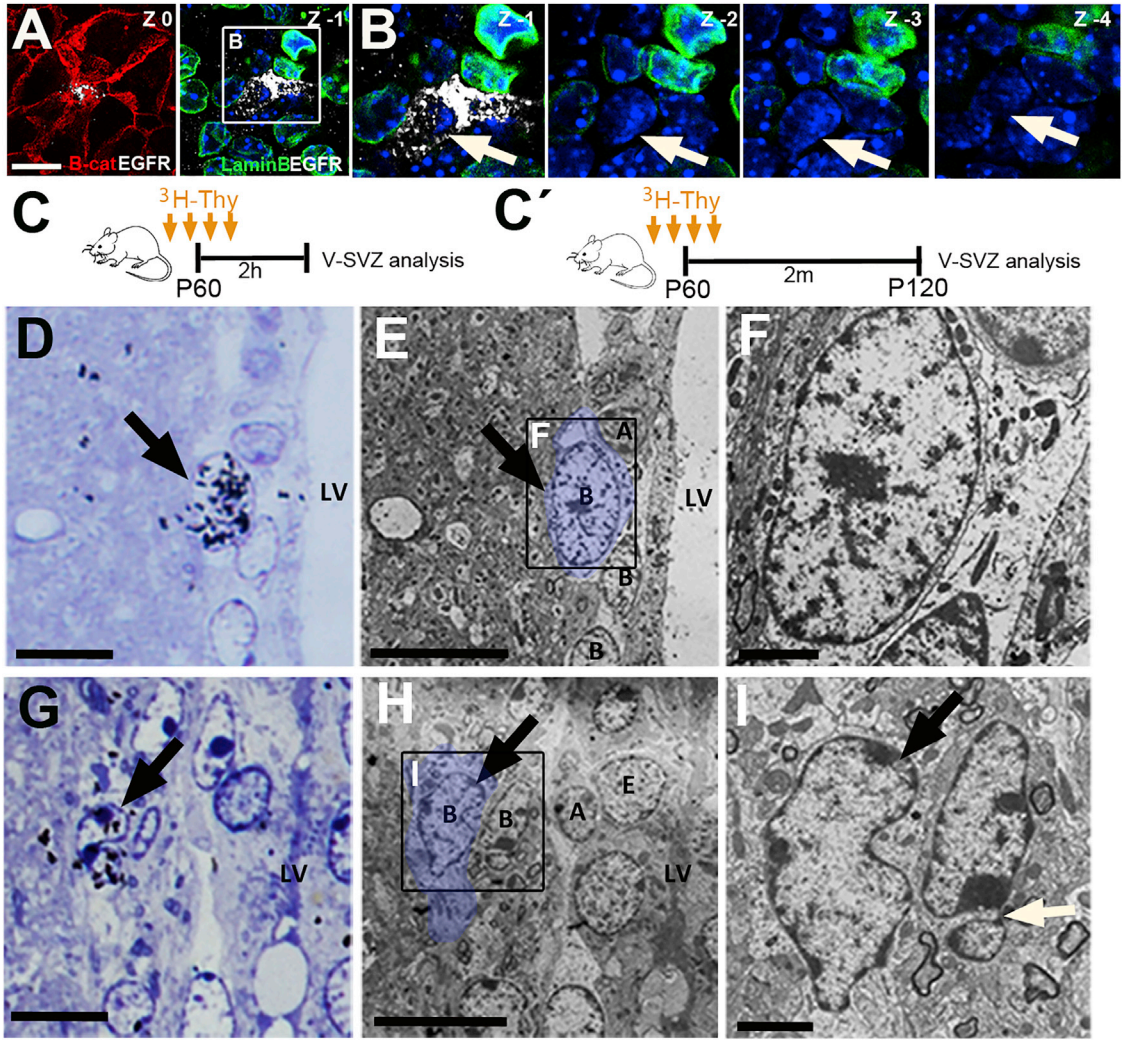

Figure 3. V-SVZ B Cells with Nuclear ELCS Are qNSCs

(A and B) Confocal images of a V-SVZ whole mount immunostained for β-catenin (red), EGFR (white), and Lamin B (green) showing an $EGFR^+$ (activated) NSC, which does not express Lamin B staining. (B) Insets show more superficial and deep z slices of the $EGFR^+$ cell nucleus. Note that this cell is negative for Lamin B (white arrows).

(C and C′) ^{3}H-Thy injection protocols. P60 animals received four ^{3}H-Thy injections and the V-SVZ was studied 2 hr and 2 months after the last injection.

(D–F) Autoradiography of the V-SVZ of a P60 mouse. (D) Labeled cells were identified on toluidine blue-stained semithin sections (arrow). (E and F) TEM micrographs of the ^{3}H-Thy-labeled cell in (D), characterized as B cell with spherical nucleus and condensed chromatin.

(G–I) Autoradiography of the V-SVZ of a P120 mouse. (G) Labeled cells were identified (arrow). (H and I) TEM micrographs of the ^{3}H-Thy-labeled cell in (G), characterized as B cell with irregular nucleus and clumps of chromatin (black arrow). Note that the ^{3}H-Thy-labeled cell does not show nuclear ELCS compared with the non-labeled B cell (white arrow).

Scale bars, 10 μm (A, D, H, E, G) and 2 μm (I, F). A, A cell; B, B cell; E, ependymal cell; LV, lateral ventricle.

rare; of >8,000 cells studied, only 20 labeled cells were observed. All LRCs had characteristics of B cells. Three-dimensional nuclear reconstruction of these LRCs showed no evidence of nuclear ELCS (Figures 3G–3I). This suggests that ELCS do not form in B cells after having divided 2 months earlier.

Antimitotic treatment with Ara-C induces the death of actively dividing V-SVZ progenitors, but qNSCs are spared (Doetsch et al., 1999; Morshead et al., 1994; Pastrana et al., 2009). We therefore tested whether cells that are retained 12 hr after a 6-day Ara-C treatment had ELCS in their nuclei. After Ara-C, fewer B cells were observed in the V-SVZ

Please cite this article in press as: Cebrián-Silla et al., Unique Organization of the Nuclear Envelope in the Post-natal Quiescent Neural Stem Cells, Stem Cell Reports (2017), http://dx.doi.org/10.1016/j.stemcr.2017.05.024

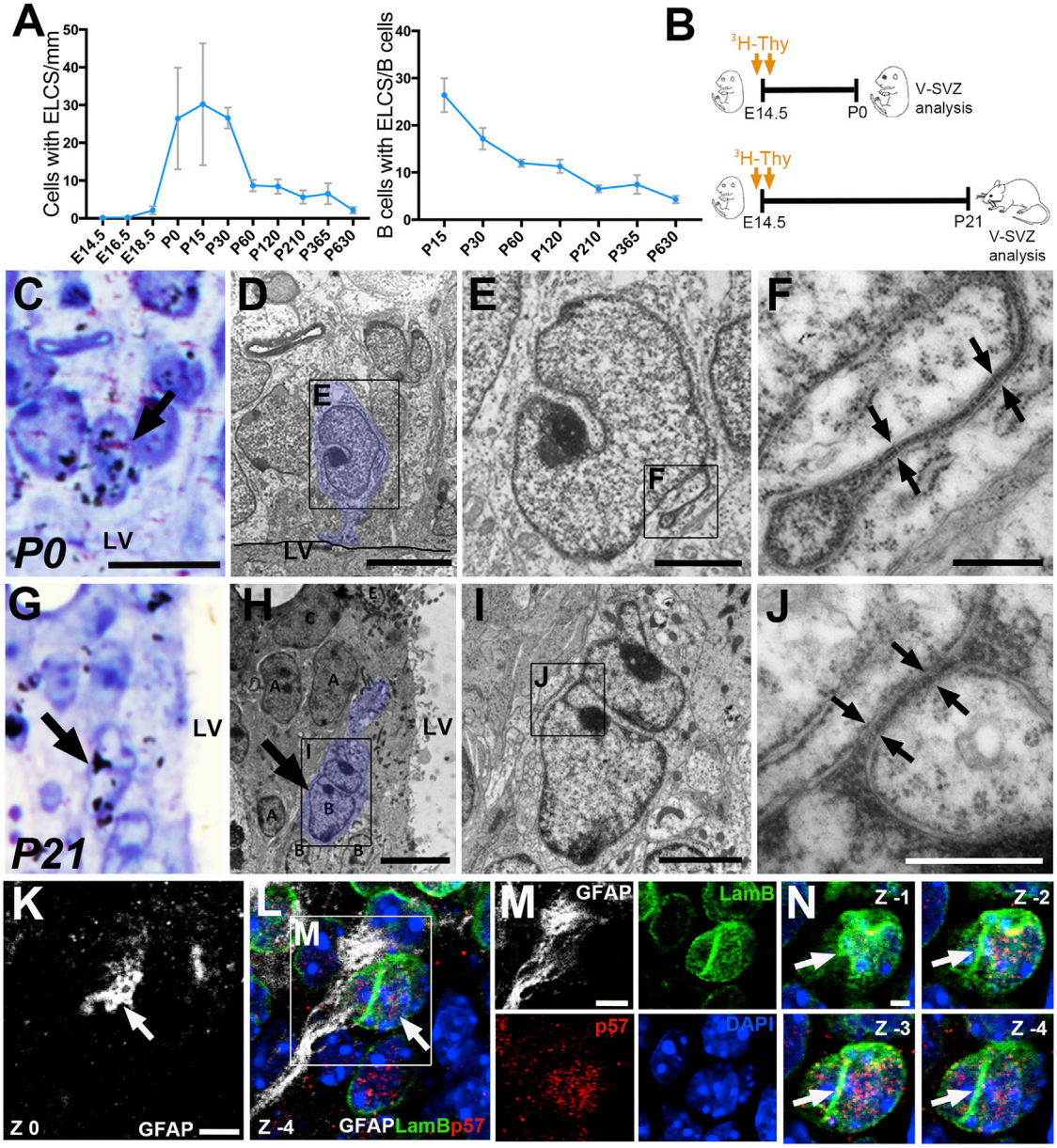

Figure 4. V-SVZ B Cells with ELCS Derive from Quiescent Pre-B1 Cells

(A) Quantifications of V-SVZ cells showing the number of cells with ELCS per millimeter at different embryonic and post-natal stages, and the percentage of B cells with ELCS/B cells at post-natal stages where B cells can be identified. Note that cells with ELCS first appear in RGCs at E14.5 with 0.14 ± 0.14 cells/mm (n = 3 mice), but its number increased progressively to an average of 30.63 ± 9.33 B cells with ELCS/mm at P15 (n = 3 mice) and then decreased at P60. Over the total population of post-natal B cells, the percentage of B cells dramatically decreases from 11.98% ± 0.43% at P60 (1,052 cells; n = 3 mice) to 4.24% ± 0.45% (466 cells; n = 3 mice) (test for trend, $p < 0.001$). Error bars represent the mean ± SEM.

(B) Diagram describing ^{3}H-Thy injection protocols. E14.5 timed pregnant mice received two ^{3}H-Thy injections and the V-SVZ of the offspring was analyzed at P0 and P21.

(C–F) Autoradiography of the V-SVZ of a P0 mouse. (C) Labeled cells were identified on toluidine blue-stained semithin sections (arrow). (D–F) TEM micrographs of the ^{3}H-Thy-labeled cell in (C). Note that this cell shows RG cell characteristics, contacts the LV, and shows nuclear ELCS (arrows).

(legend continued on next page)

(from 80 ± 5 to 32 ± 10; t test $p < 0.05$; n = 3), but the percentage of B cells with ELCS increased (from 11.9% ± 0.4% to 18% ± 1%; t test, $p < 0.05$; 703 cells, n = 3). This indicates that B cells with ELCS are spared by Ara-C treatment. Fourteen days after Ara-C treatment the percentage of B cells with ELCS cells was reduced (15% ± 2%; 933 cells, n = 3). These results indicate that B cells with ELCS survive Ara-C treatment, consistent with the interpretation that they correspond to qNSCs.

Nuclear ELCS Are Not Observed In Vitro

Previous studies have shown that V-SVZ progenitors can be grown in vitro as neurospheres or in monolayer cultures (Reynolds and Weiss, 1992; Scheffler et al., 2005). Some of these in vitro NSCs maintain pluripotency and self-renewal potential. We investigated whether cells grown as neurospheres or in monolayer cultures, supplemented with EGF and fibroblast growth factor, presented ELCS in their nuclei. We studied neurosphere cells (1,550 cells, ten neurospheres; n = 5) and monolayer cells (1,000 cells, three wells, n = 5), but did not find any ELCS under either culture condition. As retinoic acid stimulation has been shown to promote ELCS formation in neutrophils (Olins et al., 1998), we treated neurosphere cultures with 2, 5, and 10 μM retinoic acid but could not find any evidence of ELCS formation in this in vitro NSC condition (500 cells; n = 6). We conclude that NSCs grown in vitro as neurospheres or in monolayer cultures do not exhibit ELCS.

Nuclear ELCS Begin Forming in the Embryo

Subsequently, we investigated at which developmental stage nuclear ELCS first appear. During embryonic development, the walls of the LVs are lined by radial glial cells (RGCs), some of which later give rise to adult V-SVZ B cells (Kriegstein and Alvarez-Buylla, 2009; Merkle et al., 2004). Using TEM, we serially sectioned and scanned RGC nuclei to look for the presence of ELCS at four embryonic stages (E10.5, E14.5, E16.5, and E18.5) and at four post-natal ages (P0, P15, P30, and P60). Although ELCS were rarely observed in RGC nuclei at E14.5 (0.1 ± 0.1 cells with ELCS/mm; n = 3), their number increased progressively through the embryonic stages to an average of 31 ± 9 B cells with ELCS/mm at P15 (n = 3), but then decreased at P60 (Figure 4A). These observations indicate that nuclear ELCS appear as early as E14.5, and are preserved in a subpopulation of adult V-SVZ.

We also studied older mice (P120, P210, P365, and P630) to determine the prevalence of ELCS in B cells with aging. Cells with ELCS were dramatically reduced from 8.7 ± 0.9 cells/mm at P60 (n = 3) to 2.1 ± 0.1 cells/mm at P630 (n = 3) (test for trend, $p < 0.02$; Figure 4A) and from 11.9% ± 0.4% at P60 (1,052 cells; n = 3) to 4.2% ± 0.5% (466 cells; n = 3) over the B cell population (test for trend, $p < 0.001$; Figure 4A). As in younger adults, complete 3D nuclear reconstructions at P630 showed a higher percentage of B cells containing ELCS (24% ± 4%; 40 cells, n = 3), still confirming a sharp decrease with aging. Moreover, ELCS length was slightly reduced from 0.4 to 2.0 μm at P60 (50 cells; n = 3) to 0.2–1.6 μm in aged B cells (P630; studied in 54 cells from three mice; not significant).

To further investigate whether cells with nuclear ELCS in post-natal stages were directly derived from pre-B1 cells (Fuentealba et al., 2015; Furutachi et al., 2015), we injected timed pregnant mice at E14.5 stage with ^{3}H-Thy (two injections 12 hr apart) and euthanized the offspring at postnatal stages P0 and P21 (Figure 4B). Serial 1.5-μm sections were studied at different rostrocaudal levels of the V-SVZ and ^{3}H-Thy-labeled cells close to the LV were serially reconstructed. Interestingly, we found that more than half of the radial glial (RG) LRCs at P0 (10 out of 15 studied cells; n = 3) and all labeled B cells at P21 (13 out of 13 studied cells; n = 3) presented ELCS in their nuclei (Figures 4C–4J, respectively). These results suggest that ELCS are assembled in pre-B1 cells in the embryo and remain in the quiescent progenitors during the transition from RG to B cells.

Next we studied the expression of p57, a recently described marker present in dividing embryonic NPCs and adult V-SVZ qNSCs (Furutachi et al., 2015). This protein is a component of the CIP/KIP family of cyclin-dependent kinase (CDK) inhibitory proteins, related to the blockade of cell-cycle progression by binding and inhibiting cyclin/CDK complexes of the G_1 phase (Tury et al., 2012). We analyzed the expression of p57 in the V-SVZ of embryonic and P60 mice using confocal microscopy. B cells showing NE folding, consistent with the presence of ELCS, were positive for $p57^{+}$ (25/30 of P60 and 18/24 of E18) (Figures 4K–4N and S3). Taken together, these results indicate that nuclear ELCS is a hallmark of V-SVZ qNSCs derived from pre-B1 cells.

Formation of ELCS during Development

Since nuclear ELCS start forming in some RGCs at E14.5, we performed a serial ultrastructural analysis of RGC

(G–J) Autoradiography of the V-SVZ of a P21 mouse. (G) Labeled cells were identified on toluidine blue-stained semithin sections (arrow). (H–J) Electron micrographs of the ^{3}H-Thy-labeled cell shown in (G). Note that this cell is characterized as a B cell and shows nuclear ELCS (arrows).

(K–N) Confocal images of a V-SVZ whole mount immunostained for GFAP (white), Lamin B (green), and p57 (red) to visualize B1 cells with ELCS nuclear expression of p57. Note that the insets (N) show the characteristic ELCS zone (white arrows) and co-localization with p57. Scale bars, 10 μm (C, D), 5 μm (K, M), 2 μm (E, H, I, N), and 500 nm (F, J).

Please cite this article in press as: Cebrián-Silla et al., Unique Organization of the Nuclear Envelope in the Post-natal Quiescent Neural Stem Cells, Stem Cell Reports (2017), http://dx.doi.org/10.1016/j.stemcr.2017.05.024

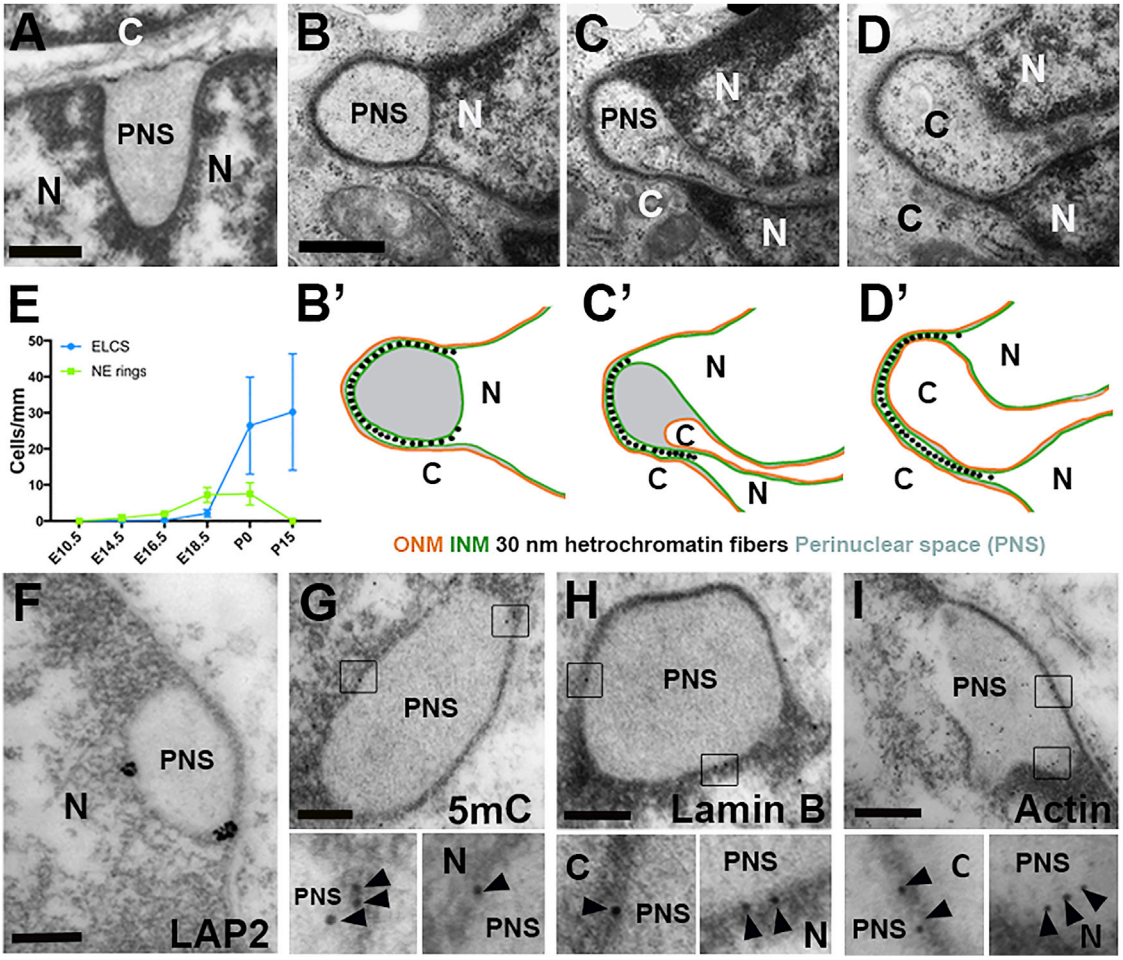

Figure 5. Nuclear ELCS Formation and Components

(A) TEM micrograph of an RGC nucleus showing a punctual detachment of the INM and ONM, generating an increment of the PNS.

(B–D′) TEM serial sections and their schematics showing that the ONM aligned to the INM reducing the PNS, and likely generating ELCS (see Figure S1 for complete series of sections).

(E) TEM quantification of the number of cells with ELCS (blue) or NE rings (green) per millimeter (n = 3 mice). Note that the number of cells with NE rings is 0 at P15, which coincides with the maximum peak of cells containing ELCS at this age (30.21 cells with ELCS/mm; n = 3 mice). Error bars represent the mean ± SEM.

(F–I) Pre- and post-embedding immunogold staining for Lap2 (F), 5mC (G), Lamin B (H), and actin (I) in E18 VZ RG cells. Arrowheads indicate gold particles associated to each staining.

Scale bars, 500 nm (A, B; applies also to C, D) and 200 nm (F–I). C, cytoplasm; N, nucleus; PNS, perinuclear space.

nuclear morphology by TEM at different stages of embryonic development. Punctual detachments of the INM and ONM were observed in some RGCs (from E14.5 to P0). This resulted in an increased perinuclear space in the detachment zone (Figures 5A–5E). On tangential sections, this NE detachment appeared as a perinuclear space sphere. Hence, we refer to this structure as the "nuclear envelope ring" (NE ring). The ONM was clearly distinguished by its attached ribosomes and the INM by the presence of nuclear lamina. To characterize the 3D organization of NE rings and to investigate their possible relation with nuclear ELCS, we performed P0 V-SVZ 3D reconstructions by TEM. As NE ring sections were stacked, we observed that the ONM aligned to the INM, reducing the perinuclear space and likely generating ELCS (six cells) (Figures 5B–5D and S4). Importantly, as ELCS, the nuclear rings were partially lined by ~30-nm chromatin fibers. These results were supported by the fact that the NE ring perinuclear space was delimited by INM marker Lap2 and heterochromatin fibers labeled by 5-methylcytosine (5mC) (Figures 5F and 5G). We also confirmed the expression of Lamin B, a main component of the type B cell NE, in the periphery of the NE rings

Please cite this article in press as: Cebrián-Silla et al., Unique Organization of the Nuclear Envelope in the Post-natal Quiescent Neural Stem Cells, Stem Cell Reports (2017), http://dx.doi.org/10.1016/j.stemcr.2017.05.024

(Figure 5H). In addition, to support that ELCS formation is a dynamic process that requires components of the nuclear cytoskeleton, we studied actin expression in NE rings (Figure 5I). Remarkably, we observed that actin was highly expressed in the perinuclear space of NE rings compared with the neighboring NE and nucleoplasm. These observations suggest that NE rings are a transitory NE structure related to the formation of nuclear ELCS during the stages E14.5 to P15.

ELCS as a Nuclear Compartment

The NE and the nuclear lamina play important roles in cell-cycle regulation as well as in genome and cytoskeletal organization (Malhas et al., 2011). They harbor tissue-specific resident proteins, extensively interact with chromatin, and contribute to spatial genome organization and regulation of gene expression (Brachner and Foisner, 2011; Las Heras de and Schirmer, 2014). Since nuclear ELCS were mainly formed by the NE, we decided to study whether components of the NE and nuclear lamina are expressed in ELCS. We performed immunogold and immunofluorescence detection of the INM proteins Lap2 and LBR, and the nuclear lamina intermediate filament Lamin B. Congruently, we found that all of these proteins were widely distributed along the NE and were also found in ELCS (Figures 6A–6C, S5A, S5B, S5D, and S5E). However, Lamin B and Lap2 were significantly more highly expressed within ELCS (t test, $p < 0.01$ for Lamin B; $p < 0.05$ for Lap2). We next determined whether the ultrastructural 30-nm condensed chromatin fibers within nuclear ELCS expressed epigenetic markers related to heterochromatin. We performed pre- and post-embedding immunogold staining for 5mC, trimethyl-histone H3 (Lys27) (H3K27me3), trimethyl-histone H3 (Lys9) (H3K9me3), and heterochromatin protein 1 (HP1), and found that while 5mC and H3K9me3 were expressed in ELCS chromatin fibers (Figures 6D, 6E, S5C, S5F, and S5G), H3K27me3 and HP1 were present in the nuclear lobes but not within ELCS (Figures 6F–6I). Given that ELCS of B cells in the V-SVZ contained heterochromatin with specific epigenetic modifications, we examined whether ELCS heterochromatin could correspond to telomeric heterochromatic domains. It has been indeed proposed that nuclear telomere positioning may influence cell longevity in quiescence (Guidi et al., 2015). TRF2, a telomere sheltering component thought to mediate telomere binding to lamins (Gonzalo and Eissenberg, 2016), was preferentially located to the NE (Figure 6J). Intriguingly, telomere-associated protein TFR2 expression was significantly higher within ELCS or in the ELCS-endpoint heterochromatin than in the rest of the nucleus (t test, $p < 0.0002$; Figures 6K–6N, S6A, and S6B). Moreover, we investigated the nuclear telomere distribution in B cells by assay using fluorescence in situ hybridization (FISH) with peptide nucleic acid (PNA-FISH). We combined the Telomere-C probe detection with the Lamin B and GFAP expression, and found that telomeres were enriched in the ELCS zone (t test, $p < 0.05$; Figures 6P–6R, S6C, and S6D). Altogether, these results suggest that ELCS represent a specific nuclear compartment housing particular heterochromatin domains.

DISCUSSION

In this study, we show that a subset of adult V-SVZ B cells have NE-limited chromatin sheets or ELCS. Using molecular markers, ^{3}H-Thy, and the antimitotic drug Ara-C, we found that B1 cells with ELCS correspond to qNSCs. TEM analysis revealed that nuclear ELCS start to appear in RGCs in the embryo around E14.5 and are present throughout adult life in a subpopulation of V-SVZ B cells. ^{3}H-Thy birth dating suggests that quiescent B cells with ELCS have an embryonic origin. We also detected the expression of epigenetic markers associated with repression and telomeres within ELCS. This structure may represent a specific nuclear compartment associated with quiescent pre-B and B cells. Our work suggests that this unique compartment of the NE is associated with quiescence and, in particular, with the subpopulation of progenitors that are set apart during embryonic development to function in the juvenile and adult brain as NSCs.

We found out that a subset of V-SVZ B cells display a nuclear structure, characterized by a thin chromatin layer bound to the inner and outer membranes. These distinct structures highly resemble the previously described ELCS in other cell types (Davies and Small, 1968; Olins et al., 2008). The ELCS we describe in post-natal qNSCs is similar to subtype 1-1 ELCS (a single chromatin sheet bound on two sides by cytoplasm) (Olins and Olins, 2009). In the CNS, ELCS have been observed in the developing human retina (Popoff and Ellsworth, 1969) and in the subcallosal zone cells during post-natal development (Wittmann et al., 2009). Outside the CNS the presence of ELCS has been mainly reported in myeloid, lymphoid (Davies and Small, 1968; Olins et al., 1998), and cancer cells (Mollo et al., 1969; Tani et al., 1971). The functional significance of ELCS remains elusive. It has been proposed that it could facilitate neutrophil functions (Rowat et al., 2013) and may also be a part of a developmental program to shut off gene activity during terminal differentiation (Sanchez and Wangh, 1999). Remarkably, tumor cells with ELCS survive to radiation and antimitotic treatments (Ahearn et al., 1967; Erenpreisa et al., 2002; Stalzer et al., 1965), suggesting that ELCS may be present in quiescent cancer cells. Further research is needed to determine the function of ELCS. Our observations are in line with the idea that

Please cite this article in press as: Cebrián-Silla et al., Unique Organization of the Nuclear Envelope in the Post-natal Quiescent Neural Stem Cells, Stem Cell Reports (2017), http://dx.doi.org/10.1016/j.stemcr.2017.05.024

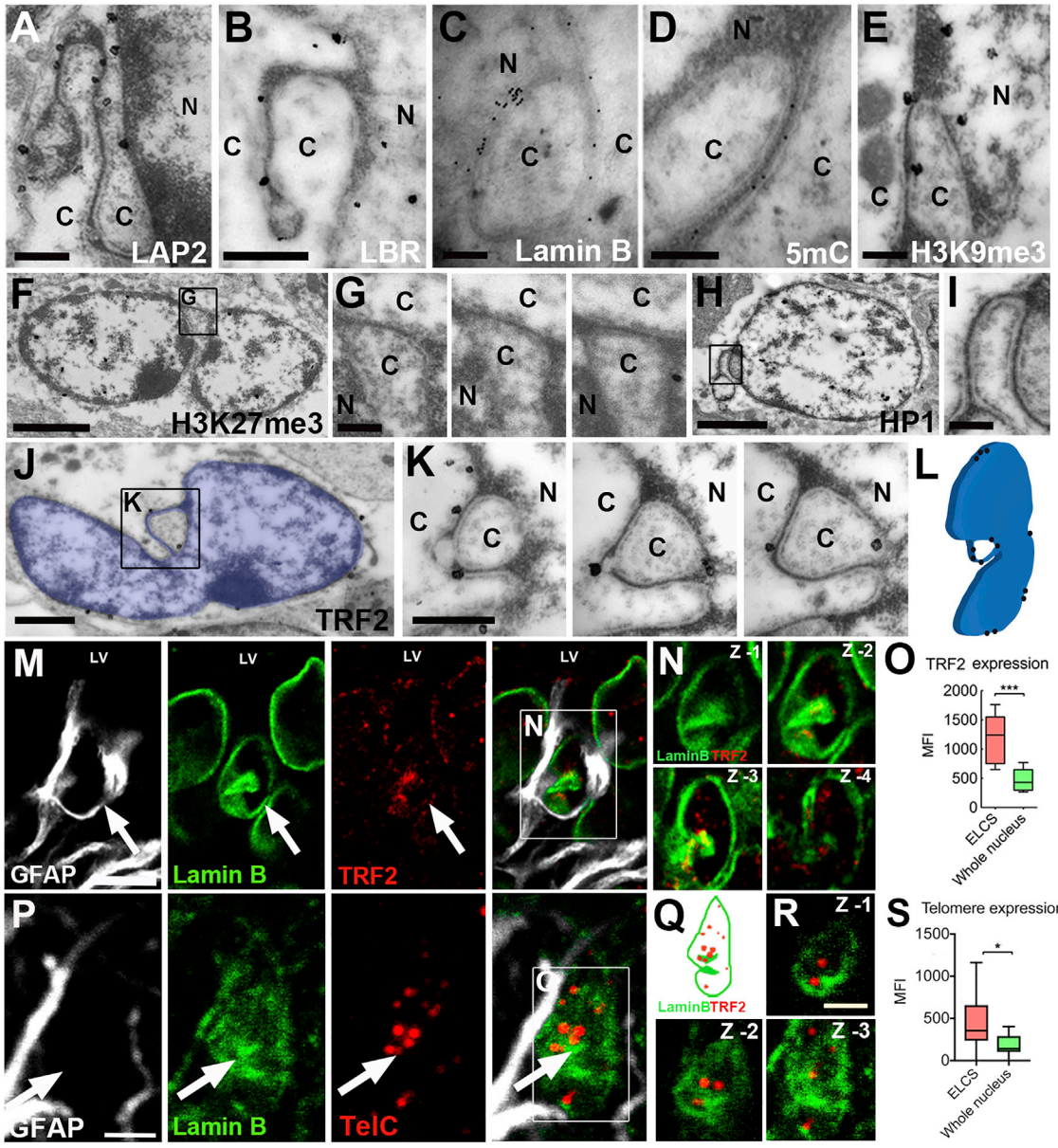

Figure 6. ELCS as a Nuclear Compartment

(A–E) Pre- and post-embedding immunogold staining for Lap2 (A), LBR (B), Lamin B (C), 5mC (D), and H3K9me3 (E) within 2-month-old V-SVZ B cell ELCS.

(F and G) Immunogold labeling for H3K27me3. H3K27me3 is present in the B cell nuclear lobes but not within ELCS in three serial ultrathin sections.

(H and I) Immunostaining for HP1 showing labeling in the nuclear lobe but not within ELCS.

(J) TRF2 pre-embedding TEM pseudo-colored image of B cell with ELCS showing the nucleus in blue and the gold labeling preferentially located in the NE periphery.

(K) High-magnification serial sections of boxed region in (J) showing that TRF2 is located within ELCS.

(L) Schematic representation of TRF2-labeled nucleus in (F) in three ultrathin sections. Note that TRF2 is highly expressed within ELCS or its boundaries.

(M–O) Confocal microscopy reveals GFAP^{+} cells contacting the LV (arrows indicate the nuclei of the cells of interest). TRF2 fluorescence is concentrated in ELCS zone, visualized as a Lamin B-labeled irregular NE (***$p < 0.001$, unpaired t test; mean ± SEM; 10 cells; n = 3 mice). Error bars represent the mean ± SEM.

(legend continued on next page)

ELCS are linked to genomic rearrangements associated with quiescence in NSCs.

Adult V-SVZ NSCs are a heterogeneous population of primary progenitors that can exist in either quiescent or activated state (Codega et al., 2014; Llorens-Bobadilla et al., 2015; Morshead et al., 1994). We found that B cells with ELCS are GFAP$^+$, BLBP$^+$, Glast$^+$, Nestin$^-$, and EGFR$^-$, do not incorporate ^{3}H-Thy, and survive following Ara-C treatment. These data suggest that ELCS are present in qNSCs. In addition, 83% of B1 cells have nuclear ELCS in contrast to the rest present a more spherical nucleus devoid of ELCS. This is consistent with previous observations reporting that 11.4% ± 1.3% of B1 cells are EGFR$^+$ and correspond to aNSCs (Codega et al., 2014) while about 8.6% are actively dividing (Ponti et al., 2013). Transcriptomic analyses have suggested that qNSCs or dormant cells enter a primed-quiescent state before activation (Llorens-Bobadilla et al., 2015; Shin et al., 2015). However, due to the dynamic nature of this process, this intermediate state has not yet been well characterized by molecular or morphological characteristics. At present we cannot conclude whether B cells with ELCS include dormant qNSCs or only primed-quiescent cells, or a subpopulation of these. Future studies might help to unravel this question.

We also observed that 2 months after ^{3}H-Thy incorporation, none of the V-SVZ LRCs exhibited ELCS in their nuclei. The number of cells exhibiting ELCS greatly decreased with age. Consistently, other reports have shown a decrease in the neurogenic potential with age (Bouab et al., 2011; Capilla-Gonzalez et al., 2014; Encinas et al., 2011). Furthermore, a recent study using barcode lineage tracing indicates that new neurons arise from distinct B1 cohorts formed in the embryo (Fuentealba et al., 2015), suggesting that B1 cells become depleted with age. The observed decrease in the number of V-SVZ cells with ELCS could be associated to a depletion of NSCs in this neurogenic niche.

We could not find any cells with ELCS under TEM when V-SVZ progenitors were expanded in vitro as neurospheres or in monolayer cultures. Previous studies have shown that cultured NSCs cells are mainly derived from actively dividing cells in vivo (Codega et al., 2014; Doetsch et al., 2002; Mich et al., 2014) which, as we showed, lack ELCS. Nevertheless, it is also possible that the qNSC induction of proliferation in culture could result in the disassembly of ELCS.

Recently, it has been suggested that yeast quiescent cells that sustain long-term viability form a discrete subcompartment of telomere silent chromatin (Guidi et al., 2015). This encouraged us to investigate whether ELCS are enriched in telomeric components. Using stainings for TRF2 and telomere FISH, we found that some telomeres are preferentially located within ELCS and their immediate proximity. Further evidence supports the idea that telomere-associated proteins are likely to contribute to the regulation of cellular proliferative capacity (Blasco, 2002; Grammatikakis et al., 2016). Previous studies have also shown that telomeres are associated to lamins and lamin-associated proteins such as Lap2, and are rich in epigenetic modifications, as we confirm here for H3K9me3 (Gonzalo and Eissenberg, 2016). Based on these data and the presence of telomeres in the ELCS and its proximity, we propose ELCS as a nuclear compartment for specific heterochromatic domains related to the quiescent state of NSCs in the V-SVZ. As molecular components of ELCS are identified, this may permit new studies about the stability of these nuclear structures. Furthermore, components of the ELCS may be employed for lineage tracing of cells within the NSC lineage.

EXPERIMENTAL PROCEDURES

Animal Samples

Mice maintenance and experimental procedures were approved by the Committee for Animal Welfare of the University of Valencia (2015/VSC/PEA/00,068), following the guidelines of the EC Directive 2010/63/UE. Wild-type CD1 mice were obtained from Charles River Laboratories.

[^{3}H]Thymidine Administration

To identify proliferating cells by TEM, we administered four intraperitoneal injections of ^{3}H-Thy at 2-hr intervals to adult mice (1.67 μL/g body weight, specific activity 5 Ci/mmol; PerkinElmer) with subsequent perfusion 2 hr after the last injection (n = 3). To detect LRCs, we injected ^{3}H-Thy as above, but perfused the animals after a 2-month survival period (n = 3). For qNSC labeling during the embryonic stages, E14.5 timed pregnant mice received two intraperitoneal injections of ^{3}H-Thy (3.34 μL/g body weight, specific activity 5 Ci/mmol; PerkinElmer) and the offspring were perfused at P0 (n = 4) and P21 (n = 4).

Ara-C Infusion

Mice brains were infused for 6 days with Ara-C (Sigma) using osmotic pumps (Alzet). The V-SVZ were dissected 0 hr after treatment for whole-mount analysis, and 12 hr and 14 days after for TEM analysis and quantifications (n = 3).

(P–S) Co-localization of GFAP and Lamin B immunofluorescence with the expression of the Telomere PNA-FISH probe (arrows) showing the preferential location of telomeres in the ELCS zone (*p < 0.05, unpaired t test; mean ± SEM; 10 cells; n = 3 mice). (P and Q) 3-μm z stack of the B cell. (R) Three serial single slices of the cell depicted in (P) are shown. (S) Error bars represent the mean ± SEM.
Scale bars, 2 μm (F, H, M, P, R), 650 nm (K), 500 nm (B, G, I), 1 μm (J), 400 nm (A), and 200 nm (C–E). C, cytoplasm; N, nucleus.

Transmission Electron Microscopy

For TEM, mice were fixed as described in Supplemental Experimental Procedures. Brains were rinsed in 0.1 M phosphate buffer (PB) and cut into 200-μm sections. Sections were post-fixed in 2% osmium tetroxide, dehydrated, and embedded in Durcupan resin (Fluka; Sigma-Aldrich). Semithin sections (1.5 μm) were cut with a diamond knife and stained with 1% toluidine blue for light microscopy. Ultrathin sections (70–80 nm) were cut, stained with lead citrate, and examined under an FEI Tecnai G^2 Spirit transmission electron microscope (FEI Europe) using a digital camera (Morada Soft Imaging System; Olympus). For pre- and post-embedding immunogold stainings, mice were perfused with 4% paraformaldehyde (PFA)/0.5% glutaraldehyde. Pre-embedding immunogold stainings were carried out as previously described (Sirerol-Piquer et al., 2012). Post-embedding immunogold stainings are described in Supplemental Experimental Procedures.

Autoradiography

Brains injected with ^{3}H-Thy were processed for TEM as described above. Subsequently, V-SVZ semithin sections were dipped in autoradiography emulsion (Carestream Autoradiography Emulsion, Type NTB), dried in the dark, and stored at 4°C for 4 weeks (Doetsch et al., 1997). Autoradiography was developed using standard methods and counterstained with 1% toluidine blue. Close to the LV ^{3}H-Thy-labeled nuclei were identified in semithin sections. Six or more silver grains needed to be present over the nucleus, and the nucleus had to be labeled in at least three consecutive serial sections, for a cell to be considered labeled. All consecutive sections showing labeled cells were selected under a light microscope (Eclipse; Nikon), re-embedded, and ultrathin-sectioned for TEM serial reconstruction. The number of ^{3}H-Thy-labeled studied cells is detailed in Supplemental Experimental Procedures.

Immunohistochemistry

Primary and secondary antibodies were incubated in PB with 0.2% Triton X-100, 5% normal goat serum, and 10% casein. Confocal images were taken on an FV1000 microscope and images were analyzed with the Olympus FV1000 software and processed with Adobe Photoshop. Fluorescence quantifications were carried out as mean gray values of the studied areas using FIJI software (Schindelin et al., 2012). An antibody list is provided in Supplemental Experimental Procedures.

Immuno-FISH

Mice (n = 3) were perfused with 4% PFA. Antigen retrieval was performed in 3-μm paraffin sections (1:200 Immunosaver; 64142, EMS). Samples were incubated with 0.005% Proteinase K (S3020, Dako) for 4 min, washed in PBS, dehydrated in cold ethanol series, and dried in air. The probe TelC-Cy3 (800 ng/mL; F1002, Discovery Peptides) was incubated 1.5 hr and washed with stringent 60× wash solution (K5201, Dako) for 15 min at 57°C. For immuno-FISH, samples were washed with PB, 0.5% BSA, and 0.1% Triton X-100, and incubated with the primary and secondary antibodies.

In Vitro Assays

Mouse V-SVZ neurosphere cultures and monolayer cultures were carried out as described in Supplemental Experimental Procedures. Cells obtained from these cultures were fixed with 3% glutaraldehyde and processed for TEM.

Quantification and Nuclear Three-Dimensionalization

Identification and quantification of V-SVZ cells under TEM was performed according the ultrastructural characterization described in Doetsch et al. (1997). For quantifications of RG with ELCS and/or with NE rings in embryonic stages (Figures 4A and 5E), cells within the VZ (first 40 μm adjacent to the ventricle lumen) were studied. For 3D nuclear reconstructions of V-SVZ cells we photographed every ultrathin section (Figure 1E; see also Movie S1). Digital electron micrographs from each level were aligned with FIJI TrakEM2 software (Saalfeld et al., 2012) and rendered with the Reconstruct software (Fiala, 2005).

Statistics

All results shown in the graphs are expressed as mean ± SEM. The means of experimental groups and fluorescence intensity were compared by unpaired two-tailed Student's t test. The decrease of B cells with ELCS with aging was evaluated by the trend test. All tests were performed using Prism 7 software (GraphPad). Differences were considered significant at $p < 0.05$.

SUPPLEMENTAL INFORMATION

Supplemental Information includes Supplemental Experimental Procedures, six figures, and one movie and can be found with this article online at http://dx.doi.org/10.1016/j.stemcr.2017.05.024.

AUTHOR CONTRIBUTIONS

Conceptualization, A.C.-S. and J.M.G.-V.; Methodology, A.C.-S., C.A.-C., V.H.-P., N.K., and D.H.P.; Writing – Original Draft, A.C.-S., C.A.-C., V.H.-P., and J.M.G.-V.; Writing – Review & Editing, D.A.L., A.A.-B., K.S., and J.M.G.-V.; Funding Acquisition, J.M.G.-V.; Supervision, D.A.L., A.A.-B., K.S., and J.M.G.-V.

ACKNOWLEDGMENTS

We would like to thank Dr. Harald Hermann (DKFC) for the anti-LBR antibody. We acknowledge Patricia Garcia-Tarraga and Susana Gonzalez-Granero for their technical help, and D.A.L. and A.A.-B. laboratory members for their technical advice and useful discussion. This research was supported by the Prometeo grant PROMETEOII/2014/075 and the MINECO/FEDER grant (BFU2015-64207-P). A.C.-S. was supported by the MINECO scholarship (FPU, AP-2010-4264). JSPS Program for Advancing Strategic International Networks to Accelerate the Circulation of Talented Researchers (Nagoya City University).

Received: December 27, 2016
Revised: May 17, 2017
Accepted: May 18, 2017
Published: June 22, 2017

Please cite this article in press as: Cebrián-Silla et al., Unique Organization of the Nuclear Envelope in the Post-natal Quiescent Neural Stem Cells, Stem Cell Reports (2017), http://dx.doi.org/10.1016/j.stemcr.2017.05.024

REFERENCES

Ahearn, M.J., Lewis, C.W., Campbell, L.A., and Luce, J.K. (1967). Nuclear bleb formation in human bone marrow cells during cytosine arabinoside therapy. Nature *215*, 196–197.

Alvarez-Buylla, A., Garcia-Verdugo, J.M., and Tramontin, A.D. (2001). A unified hypothesis on the lineage of neural stem cells. Nat. Rev. Neurosci. *2*, 287–293.

Blasco, M.A. (2002). Telomerase beyond telomeres. Nat. Rev. Cancer *2*, 627–633.

Bouab, M., Paliouras, G.N., Aumont, A., Forest-Bérard, K., and Fernandes, K.J.L. (2011). Aging of the subventricular zone neural stem cell niche: evidence for quiescence-associated changes between early and mid-adulthood. Neuroscience *173*, 135–149.

Brachner, A., and Foisner, R. (2011). Evolvement of LEM proteins as chromatin tethers at the nuclear periphery. Biochem. Soc. Trans. *39*, 1735–1741.

Capelson, M., and Corces, V.G. (2012). Boundary elements and nuclear organization. Biol. Cell *96*, 617–629.

Capilla-Gonzalez, V., Cebrian-Silla, A., Guerrero-Cazares, H., Garcia-Verdugo, J.-M., and Quiñones-Hinojosa, A. (2014). Age-related changes in astrocytic and ependymal cells of the subventricular zone. Glia *62*, 790–803.

Codega, P., Silva-Vargas, V., Paul, A., Maldonado-Soto, A.R., DeLeo, A.M., Pastrana, E., and Doetsch, F. (2014). Prospective identification and purification of quiescent adult neural stem cells from their in vivo niche. Neuron *82*, 545–559.

Davies, H.G., and Small, J.V. (1968). Structural units in chromatin and their orientation on membranes. Nature *217*, 1122–1125.

Doetsch, F., Garcia-Verdugo, J.M., and Alvarez-Buylla, A. (1997). Cellular composition and three-dimensional organization of the subventricular germinal zone in the adult mammalian brain. J. Neurosci. *17*, 5046–5061.

Doetsch, F., Caillé, I., Lim, D.A., Garcia-Verdugo, J.M., and Alvarez-Buylla, A. (1999). Subventricular zone astrocytes are neural stem cells in the adult mammalian brain. Cell *97*, 703–716.

Doetsch, F., Petreanu, L., Caille, I., Garcia-Verdugo, J.M., and Alvarez-Buylla, A. (2002). EGF converts transit-amplifying neurogenic precursors in the adult brain into multipotent stem cells. Neuron *36*, 1021–1034.

Encinas, J.M., Michurina, T.V., Peunova, N., Park, J.H., Tordo, J., Peterson, D.A., Fishell, G., Koulakov, A., and Enikolopov, G. (2011). Division-coupled astrocytic differentiation and age-related depletion of neural stem cells in the adult hippocampus. Stem Cell *8*, 566–579.

Erenpreisa, J., Ivanov, A., Cragg, M., Selivanova, G., and Illidge, T. (2002). Nuclear envelope-limited chromatin sheets are part of mitotic death. Histochem. Cell Biol. *117*, 243–255.

Fiala, J.C. (2005). Reconstruct: a free editor for serial section microscopy. J. Microsc. *218*, 52–61.

Fuentealba, L.C., Rompani, S.B., Parraguez, J.I., Obernier, K., Romero, R., Cepko, C.L., and Alvarez-Buylla, A. (2015). Embryonic origin of postnatal neural stem cells. Cell *161*, 1644–1655.

Furutachi, S., Miya, H., Watanabe, T., Kawai, H., Yamasaki, N., Harada, Y., Imayoshi, I., Nelson, M., Nakayama, K.I., Hirabayashi, Y., and Gotoh, Y. (2015). Slowly dividing neural progenitors are an embryonic origin of adult neural stem cells. Nat. Neurosci. *18*, 657–665.

Ghadially, F.N. (1997). Case for the panel. Mitochondrial inclusions in prostate adenocarcinoma. Ultrastruct. Pathol. *21*, 475–477.

Gonzalo, S., and Eissenberg, J.C. (2016). ScienceDirect Tying up loose ends: telomeres, genomic instability and lamins. Curr. Opin. Genet. Dev. *37*, 109–118.

Gorkin, D.U., Leung, D., and Ren, B. (2014). The 3D genome in transcriptional regulation and pluripotency. Stem Cell *14*, 762–775.

Grammatikakis, I., Zhang, P., Mattson, M.P., and Gorospe, M. (2016). The long and the short of TRF2 in neurogenesis. Cell Cycle *15*, 3026–3032.

Guerrero-Cazares, H., Gonzalez-Perez, O., Soriano-Navarro, M., Zamora-Berridi, G., Garcia-Verdugo, J.M., and Quiñones-Hinojosa, A. (2011). Cytoarchitecture of the lateral ganglionic eminence and rostral extension of the lateral ventricle in the human fetal brain. J. Comp. Neurol. *519*, 1165–1180.

Guidi, M., Ruault, M., Marbouty, M., Loïodice, I., Cournac, A., Billaudeau, C., Hocher, A., Mozziconacci, J., Koszul, R., and Taddei, A. (2015). Spatial reorganization of telomeres in long-lived quiescent cells. Genome Biol. *16*, 206.

Ito, S., Magalska, A., Alcaraz-Iborra, M., Lopez-Atalaya, J.P., Rovira, V., Contreras-Moreira, B., Lipinski, M., Olivares, R., Martinez-Hernandez, J., Ruszczycki, B., et al. (2014). Loss of neuronal 3D chromatin organization causes transcriptional and behavioural deficits related to serotonergic dysfunction. Nat. Commun. *5*, 4450.

Klempin, F., and Kempermann, G. (2007). Adult hippocampal neurogenesis and aging. Eur. Arch. Psychiatry Clin. Neurosci. *257*, 271–280.

Kriegstein, A., and Alvarez-Buylla, A. (2009). The glial nature of embryonic and adult neural stem cells. Annu. Rev. Neurosci. *32*, 149–184.

Krijger, P.H.L., Di Stefano, B., de Wit, E., Limone, F., van Oevelen, C., de Laat, W., and Graf, T. (2016). Cell-of-origin-specific 3D genome structure acquired during somatic cell reprogramming. Stem Cell *18*, 597–610.

Las Heras de, J.I., and Schirmer, E.C. (2014). The nuclear envelope and cancer: a diagnostic perspective and historical overview. Adv. Exp. Med. Biol. *773*, 5–26.

Llorens-Bobadilla, E., Zhao, S., Baser, A., Saiz-Castro, G., Zwadlo, K., and Martin-Villalba, A. (2015). Single-cell transcriptomics reveals a population of dormant neural stem cells that become activated upon brain injury. Stem Cell *17*, 329–340.

Lois, C., and Alvarez-Buylla, A. (1994). Long-distance neuronal migration in the adult mammalian brain. Science *264*, 1145–1148.

Malhas, A., Goulbourne, C., and Vaux, D.J. (2011). The nucleoplasmic reticulum: form and function. Trends Cell Biol. *21*, 362–373.

Merkle, F.T., Tramontin, A.D., Garcia-Verdugo, J.M., and Alvarez-Buylla, A. (2004). Radial glia give rise to adult neural stem cells in the subventricular zone. Proc. Natl. Acad. Sci. USA *101*, 17528–17532.

Mich, J.K., Signer, R.A., Nakada, D., Pineda, A., Burgess, R.J., Vue, T.Y., Johnson, J.E., and Morrison, S.J. (2014). Prospective identification of functionally distinct stem cells and neurosphere-initiating cells in adult mouse forebrain. Elife *3*, e02669.

Mirzadeh, Z., Merkle, F.T., Soriano-Navarro, M., Garcia-Verdugo, J.M., and Alvarez-Buylla, A. (2008). Neural stem cells confer unique pinwheel architecture to the ventricular surface in neurogenic regions of the adult brain. Stem Cell *3*, 265–278.

Mirzadeh, Z., Doetsch, F., Sawamoto, K., Wichterle, H., and Alvarez-Buylla, A. (2010). The subventricular zone en-face: whole-mount staining and ependymal flow. J. Vis. Exp., e1938. http://dx.doi.org/10.3791/1938.

Mollo, F., Canese, M.G., and Stramignoni, A. (1969). Nuclear sheets in epithelial and connective tissue cells. Nature *221*, 869–870.

Morshead, C.M., Reynolds, B.A., Craig, C.G., McBurney, M.W., Staines, W.A., Morassutti, D., Weiss, S., and van der Kooy, D. (1994). Neural stem cells in the adult mammalian forebrain: a relatively quiescent subpopulation of subependymal cells. Neuron *13*, 1071–1082.

Olins, D.E., and Olins, A.L. (2009). Nuclear envelope-limited chromatin sheets (ELCS) and heterochromatin higher order structure. Chromosoma *118*, 537–548.

Olins, A.L., Buendia, B., Herrmann, H., Lichter, P., and Olins, D.E. (1998). Retinoic acid induction of nuclear envelope-limited chromatin sheets in HL-60. Exp. Cell Res. *245*, 91–104.

Olins, A., Zwerger, M., Herrmann, H., Zentgrafg, H., Simon, A., Monestier, M., and Olins, D. (2008). The human granulocyte nucleus: unusual nuclear envelope and heterochromatin composition. Eur. J. Cell Biol. *87*, 279–290.

Pastrana, E., Cheng, L.C., and Doetsch, F. (2009). Simultaneous prospective purification of adult subventricular zone neural stem cells and their progeny. Proc. Natl. Acad. Sci. USA *106*, 6387–6392.

Peric-Hupkes, D., Meuleman, W., Pagie, L., Bruggeman, S.W.M., Solovei, I., Brugman, W., Gräf, S., Flicek, P., Kerkhoven, R.M., van Lohuizen, M., et al. (2010). Molecular maps of the reorganization of genome-nuclear lamina interactions during differentiation. Mol. Cell *38*, 603–613.

Phillips-Cremins, J.E., Sauria, M.E.G., Sanyal, A., Gerasimova, T.I., Lajoie, B.R., Bell, J.S.K., Ong, C.T., Hookway, T.A., Guo, C., Sun, Y., et al. (2013). Architectural protein subclasses shape 3D organization of genomes during lineage commitment. Cell *153*, 1281–1295.

Ponti, G., Obernier, K., Guinto, C., Jose, L., Bonfanti, L., and Alvarez-Buylla, A. (2013). Cell cycle and lineage progression of neural progenitors in the ventricular-subventricular zones of adult mice. Proc. Natl. Acad. Sci. USA *110*, E1045–E1054.

Popoff, N., and Ellsworth, R.M. (1969). The fine structure of nuclear alterations in retinoblastoma and in the developing human retina: in vivo and in vitro observations. J. Ultrastruct. Res. *29*, 535–549.

Reynolds, B.A., and Weiss, S. (1992). Generation of neurons and astrocytes from isolated cells of the adult mammalian central nervous system. Science *255*, 1707–1710.

Rowat, A.C., Jaalouk, D.E., Zwerger, M., Ung, W.L., Eydelnant, I.A., Olins, D.E., Olins, A.L., Herrmann, H., Weitz, D.A., and Lammerding, J. (2013). Nuclear envelope composition determines the ability of neutrophil-type cells to passage through micron-scale constrictions. J. Biol. Chem. *288*, 8610–8618.

Saalfeld, S., Fetter, R., Cardona, A., and Tomancak, P. (2012). Elastic volume reconstruction from series of ultra-thin microscopy sections. Nat. Methods *9*, 717–720.

Sanchez, J.A., and Wangh, L.J. (1999). New insights into the mechanisms of nuclear segmentation in human neutrophils. J. Cell. Biochem. *73*, 1–10.

Scheffler, B., Walton, N.M., Lin, D.D., Goetz, A.K., Enikolopov, G., Roper, S.N., and Steindler, D.A. (2005). Phenotypic and functional characterization of adult brain neuropoiesis. Proc. Natl. Acad. Sci. USA *102*, 9353–9358.

Schindelin, J., Arganda-Carreras, I., Frise, E., Kaynig, V., Longair, M., Pietzsch, T., Preibisch, S., Rueden, C., Saalfeld, S., Schmid, B., et al. (2012). Fiji: an open-source platform for biological-image analysis. Nat. Methods *9*, 676–682.

Seri, B., Garcia-Verdugo, J.M., Collado-Morente, L., McEwen, B.S., and Alvarez-Buylla, A. (2004). Cell types, lineage, and architecture of the germinal zone in the adult dentate gyrus. J. Comp. Neurol. *478*, 359–378.

Sexton, T., and Cavalli, G. (2013). The 3D genome shapes up for pluripotency. Stem Cell *13*, 3–4.

Shin, J., Berg, D.A., Zhu, Y., Shin, J.Y., Song, J., Bonaguidi, M.A., Enikolopov, G., Nauen, D.W., Christian, K.M., Ming, G.L., and Song, H. (2015). Single-cell RNA-seq with waterfall reveals molecular cascades underlying adult neurogenesis. Stem Cell *17*, 360–372.

Sirerol-Piquer, M.S., Cebrian-Silla, A., Alfaro-Cervelló, C., Gomez-Pinedo, U., Soriano-Navarro, M., and Verdugo, J.M.G. (2012). GFP immunogold staining, from light to electron microscopy, in mammalian cells. Micron *43*, 589–599.

Stalzer, R.C., Kiely, J.M., Pease, G.L., and Brown, A.L. (1965). Effect of 5-fluorouracil on human hematopoiesis. A morphologic study. Cancer *18*, 1071–1078.

Tani, E., Takeuchi, J., Ishijima, Y., Higashi, N., Fujihara, E., Ametani, T., and Ando, K. (1971). Elongated nuclear sheet and intranuclear myelin figure of human medulloblastoma. Cancer Res. *31*, 2120–2129.

Tavazoie, M., Van der Veken, L., Silva-Vargas, V., Louissaint, M., Colonna, L., Zaidi, B., Garcia-Verdugo, J.M., and Doetsch, F. (2008). A specialized vascular niche for adult neural stem cells. Stem Cell *3*, 279–288.

Tury, A., Mairet-Coello, G., and DiCicco-Bloom, E. (2012). The multiple roles of the cyclin-dependent kinase inhibitory protein p57KIP2 in cerebral cortical neurogenesis. Dev. Neurobio. *72*, 821–842.

Wittmann, M., Queisser, G., Eder, A., Wiegert, J.S., Bengtson, C.P., Hellwig, A., Wittum, G., and Bading, H. (2009). Synaptic activity induces dramatic changes in the geometry of the cell nucleus: interplay between nuclear structure, histone H3 phosphorylation, and nuclear calcium signaling. J. Neurosci. *29*, 14687–14700.

Stem Cell Reports, Volume *9*

Supplemental Information

Unique Organization of the Nuclear Envelope in the Post-natal Quiescent Neural Stem Cells

Arantxa Cebrián-Silla, Clara Alfaro-Cervelló, Vicente Herranz-Pérez, Naoko Kaneko, Dae Hwi Park, Kazunobu Sawamoto, Arturo Alvarez-Buylla, Daniel A. Lim, and José Manuel García-Verdugo

Supplemental Information

Supplemental Data Items

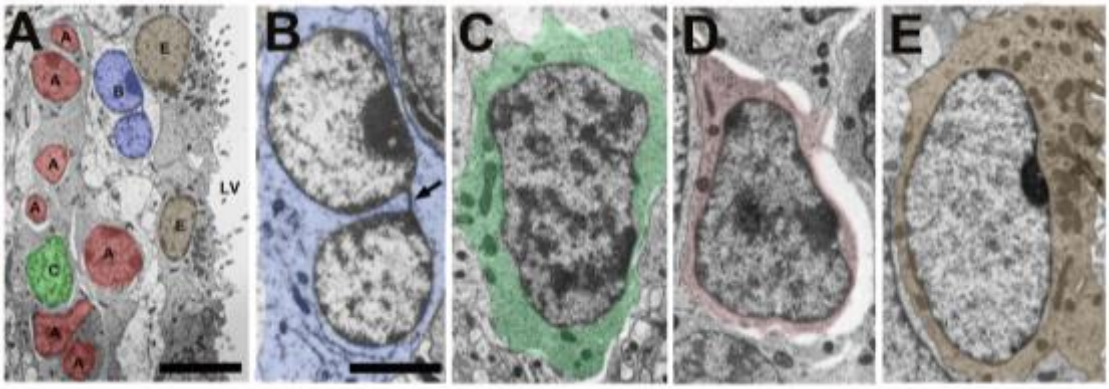

Figure S1. The V-SVZ A, C and E cell types do not show ELCS. **(A)** TEM micrograph showing the V-SVZ main cell types nuclei pseudo-colored in blue (B cell), green (C cell), red (A cells) and brown (E cells), respectively. Note that B cell shows an invaginated nucleus compared to the other cell types. **(B-E)** Higher magnification images of the V-SVZ cell types obtained from serial tridimensional reconstructions. Cytoplasm showing the typical characteristics of each cell type is pseudo-coloured in blue (B cell), green (C cell), red (A cell) and brown (E cell). Note that only B cell exhibits ELCS (arrow). Scale bars, 5 μm (A), 2 μm (B-E).

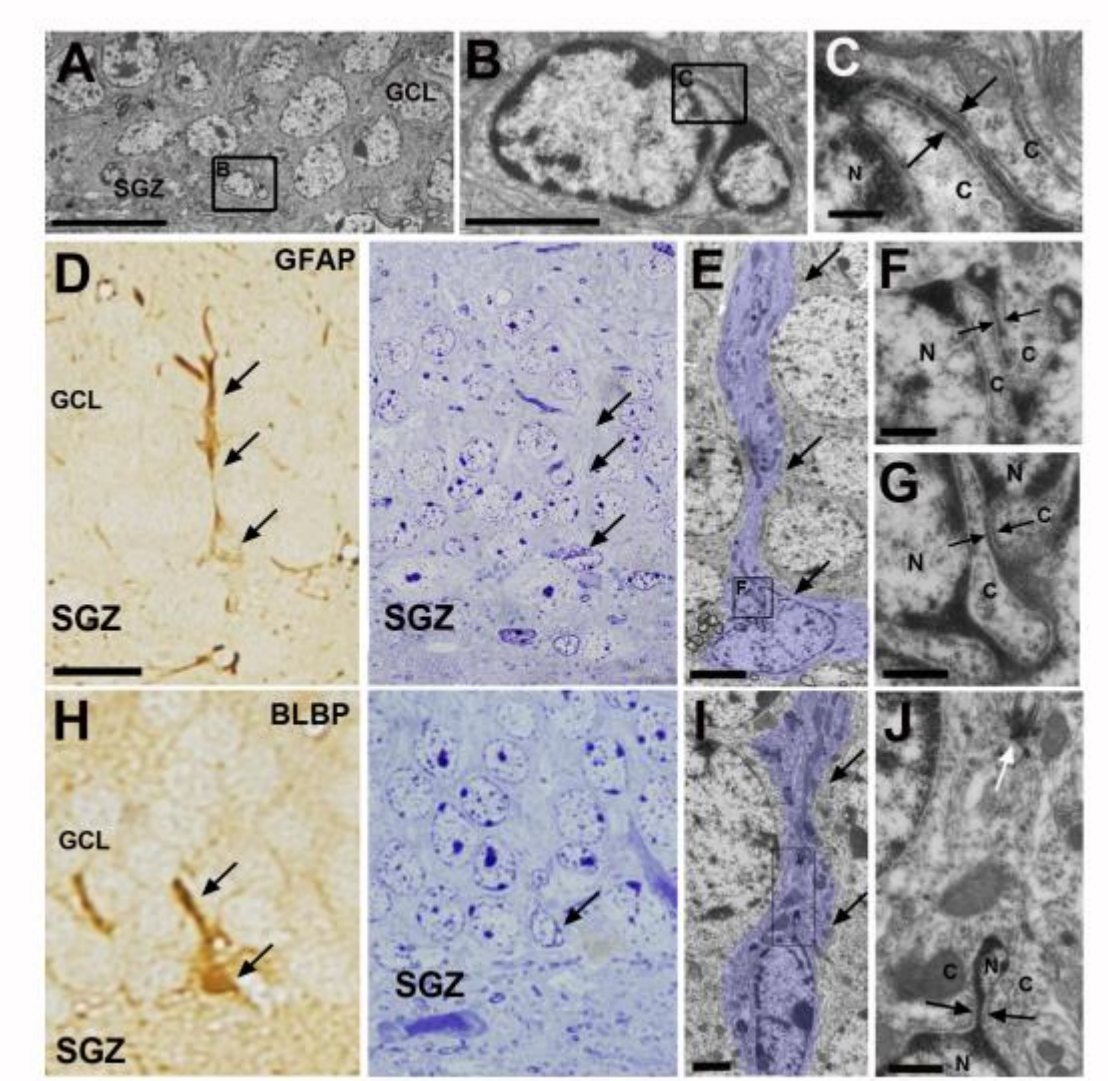

Figure S2. ELCS are present in radial astrocytes of the dentate gyrus subgranular zone. (**A-C**) TEM micrographs of an astrocyte located in the SGZ exhibiting nuclear ELCS (arrows). Scale bars, (A), 2 µm (B), 200 nm (C). SGZ: subgranular zone, GL: granular layer, N: nucleus, C: cytoplasm. (**D-J**) Post-embedding DAB immuno-detections for GFAP and BLBP. showing radial astrocytes in the SGZ. Scale bar: 50 µm. (**E, I**) TEM photomicrographs of GFAP and BLBP labeled cells in (D) and (H) respectively, showing a radial expansion through the granular layer and irregular nucleus. Scale bar, 2.5 µm (E), 1 µm (I). (F, G) Two consecutive high-magnification serial sections of the region boxed in (E) showing a detail of a nuclear ELCS. Scale bar, 500 nm (F, G). (J) High magnification of the ELCS (black arrows) and the primary cilium (white arrows). Scale bar, 500 nm (J).

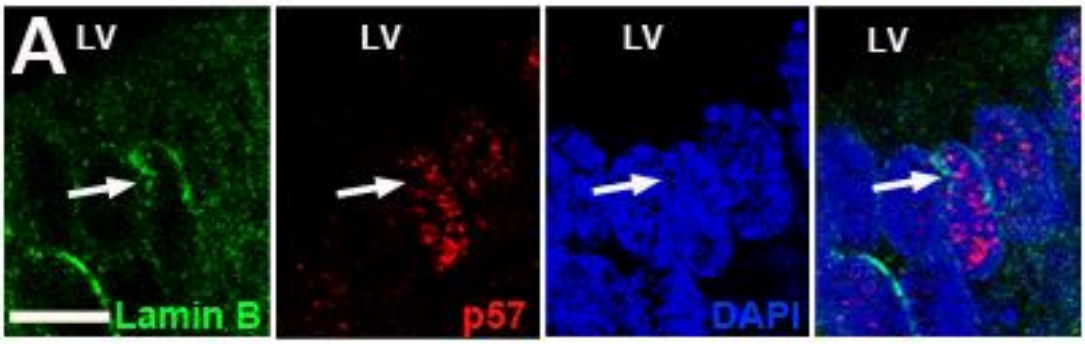

Figure S3. P57 expression in the embryo SVZ irregular nucleus. Related to Figure 4. (A) Confocal images of an E18 V-SVZ cell immunostained for Lamin B (green), p57 (red) and DAPI (blue) to visualize the nuclear expression of p57 (arrows) in cells with ELCS. Scale bar, 5 μm. LV: lateral ventricle.

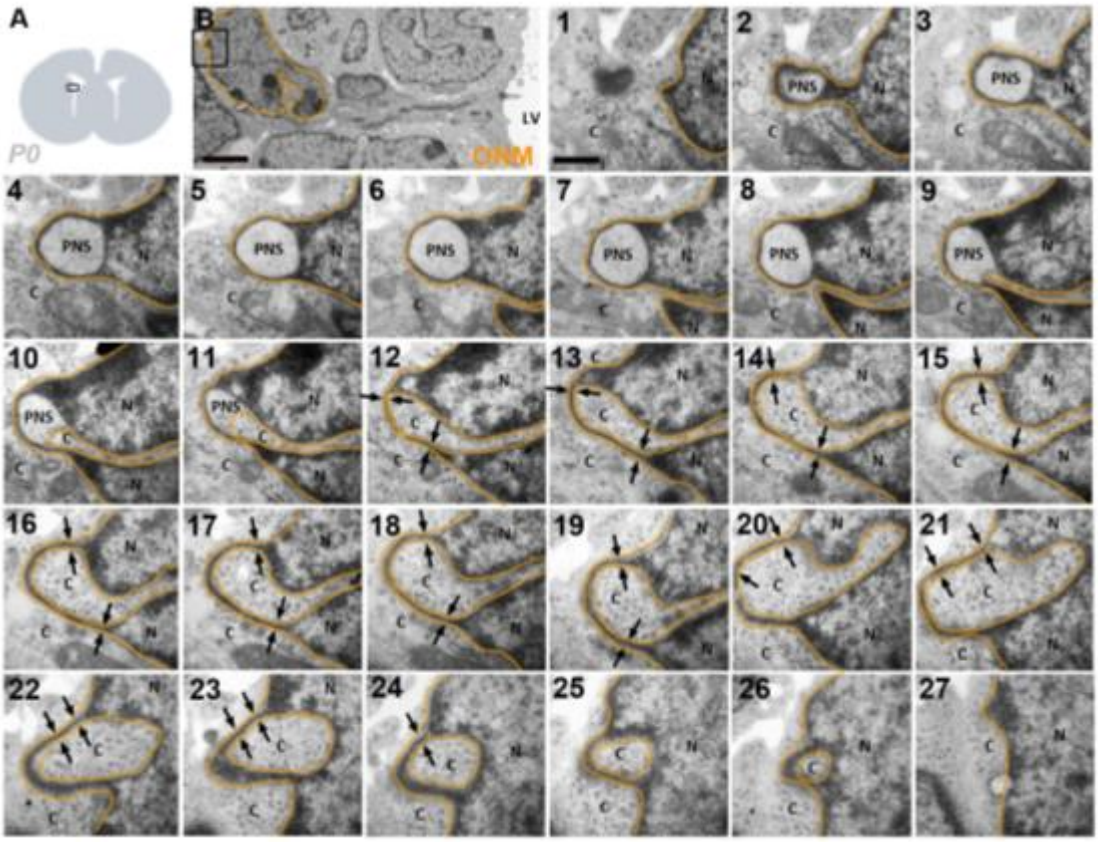

Figure S4. Link between NE rings and nuclear ELCS in RG cells. Related to Figure 5: (A) P0 mouse brain diagram indicating the V-SVZ area serially reconstructed in B. (B) TEM micrograph showing a SVZ RG cell. The ONM is outlined in orange. Scale bar, 2 μm. (1-27) High-magnification TEM serial sections of the inset region in (B). (1-11) Serial reconstruction of the NE ring showing the characteristic 30 nm layer of chromatin and dilated PNS. Note that the ONM (orange) starts to ONM aligned to the INM reducing the PNS, and likely generating ELCS in picture 9. (12-27) Arrows point to the nuclear ELCS structure with the 30 nm chromatin layer bounded into the two sides by the INM and ONM (pink). Scale bar, 500 nm. C: cytoplasm, N: nucleus, PNS: perinuclear space.

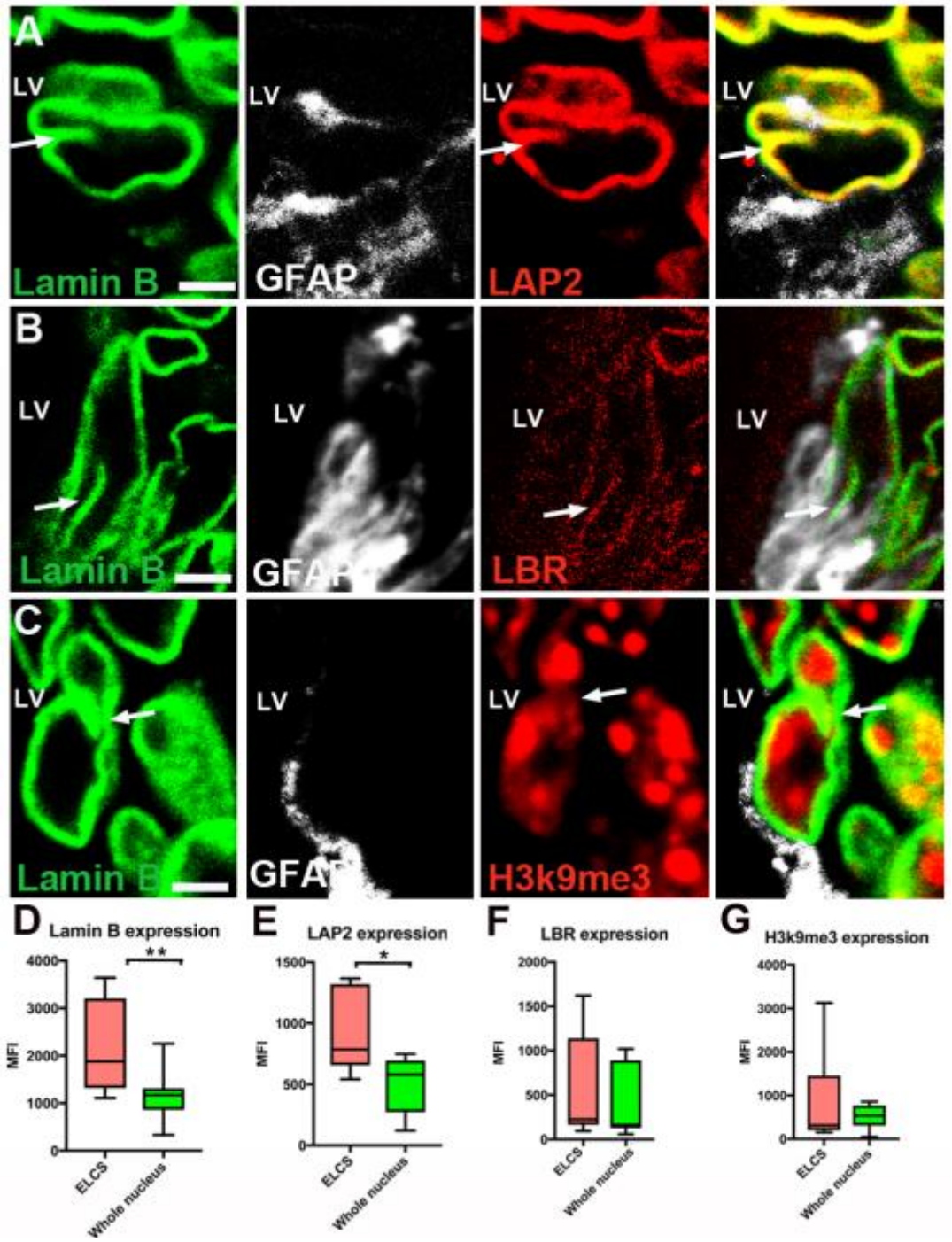

Figure S5. ELCS molecular components. Related to Figure 6: (**A-C**) Confocal images of P60 V-SVZ coronal sections immunostained for Lamin B (green), GFAP (white) and LAP2, LBR and H3k9me3 (red). Note that cells show the characteristic irregular nuclear morphology (white arrows) and co-localization with LAP2, LBR and H3k9me3. Scale bar, 2 µm (A-C). LV: lateral ventricle. (**D-G**) Mean fluorescence index (MFI) of the Lamin B, Lap2, LBR and H3k9me3 expression in the ELCS compared to the whole nucleus. Note that Lamin B and LAP2 expression are preferentially expressed within ELCS (**$p < 0.01$, unpaired t test; mean ± SEM; 10 cells; n=5 mice for Lamin B) (*$p < 0.05$; 10 cells; n=3 mice for Lap2) (ns; 10 cells; n=3 mice for LBR and H3k9me3). Data are presented as mean ± SEM.

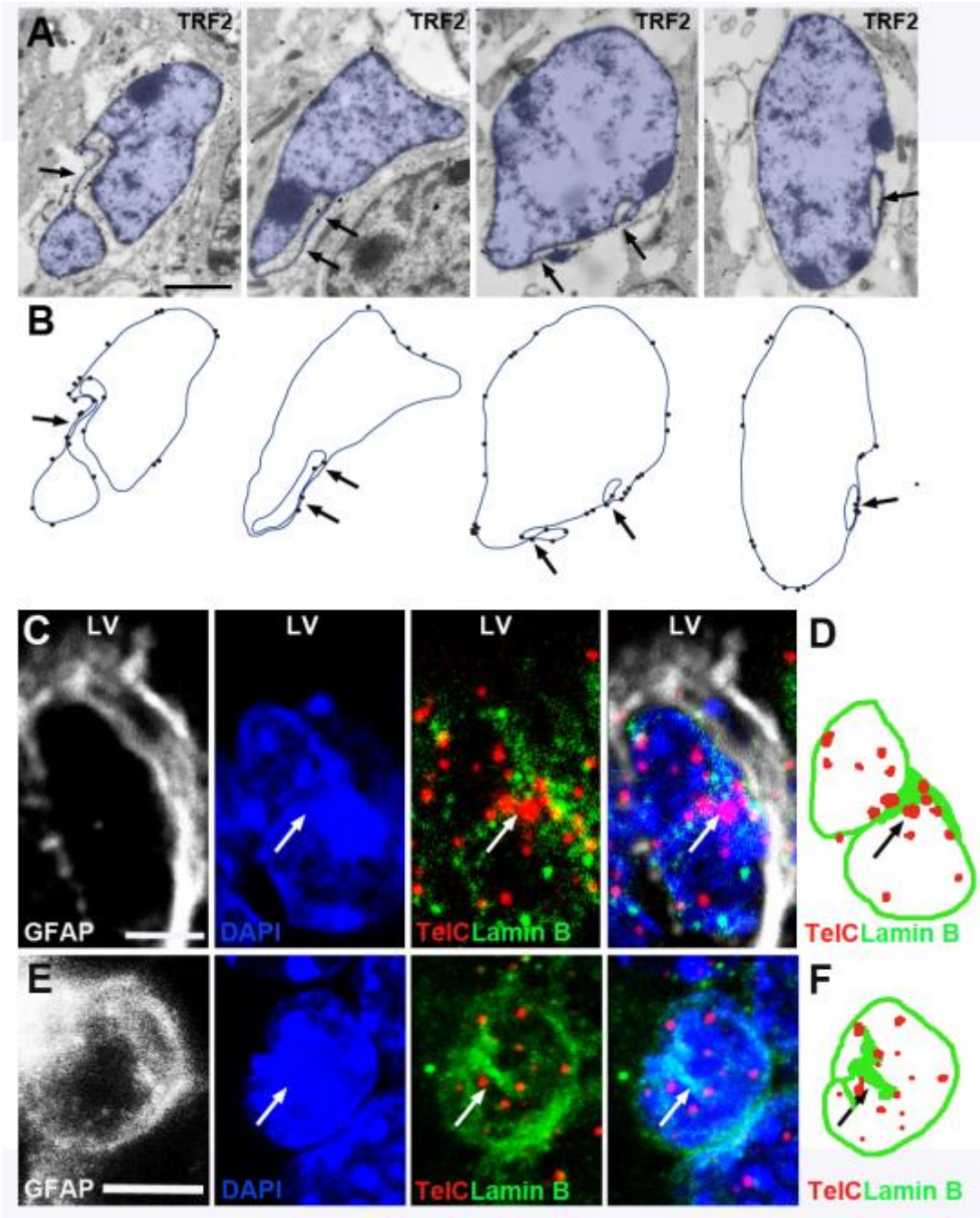

Figure S6. TRF2 and Telomere expression in V-SVZ B cells. Related to Figure 6. (**A**) TEM TRF2 pre-embedding immunogold images of type B-ELCS cells showing pseudo-colored nuclei in blue. Arrows point out ELCS (B) Schematic representation of TRF2 labeled nuclei in (C) in three ultrathin sections. Note that TRF2 labeling is highly expressed within the ELCS or its boundary. Scale bar, 2 μm (A, B). (**C, E**) Inmuno-FISH showing the telomere C distribution in a B1 cell (GFAP, white). This cell shows an irregular nucleus with ELCS (Lamin B, green)(arrows) (Image obtained from merge 5 Z stacks). (**D, F**) Schematic diagram of labeled cell in C showing preferential distribution of telomeres in the ELCS zone. Scale bar, 2 μm (C-F).

Movie S1: Type B cell with ELCS nuclear image sequence. Related to Figure 1: Type B cells with ELCS show a very irregular nucleus. ELCS are usually internalized within the nucleus.

Supplemental Experimental Procedures

Tissue Preparation

Mice were deeply anesthetized with 100 mg/Kg sodium penthobarbital (Eutanax) and perfused transcardially with saline (0.9% NaCl), followed by 4% paraformaldehyde (PFA) for immunohistochemistry, or 2% paraformaldehyde and 2.5% glutaraldehyde for electron microscopy. Brains were removed and postfixed in fresh fixative solution overnight, rinsed in 0.1 M phosphate buffer (PB). For whole mount preparation, brains were removed and the lateral walls were immediately dissected out as previously described (Mirzadeh et al., 2008). Whole mounts were fixed in 4% PFA at 4 ºC overnight and then stored in PB containing 0.1% sodium azide at 4 ºC until immunohistochemical processing.

Post-embedding immunogold staining

Ultrathin sections (70-80 nm) were cut and transferred to nickel grids. Grids were floated on top of drops of the reagents described below on a sheet of Parafilm®. In order to remove Durcupan resin, grids were incubated with 1% periodic acid for 10 min. The grids were washed on drops of H_2O 3x3 min and transferred to 2% sodium metaperiodate in H_2O for 15 min, and washed again on drops of H_2O 3x3 min. To inactivate residual aldehyde groups present after aldehyde fixation, grids were incubated on 1% sodium borohidrure in H_2O for 30 min. Subsequently, the samples were washed in 0.05 M Tris-HCl-0.9% NaCl and incubated in 1% ovoalbumin for 30 min. The grids were then transferred onto drops of a dilution of specific primary antibody for 2 hours and washed twice in 0.05 M Tris-HCl-0.9% NaCl 10 min each. Next, grids were washed once in 0.05 M Tris-HCl-0.9% NaCl with 1% bovine serum albumin (BSA) and 0.5% Tween-20 for 10 min and transferred to drops of the appropriate gold conjugate reagent (colloidal gold 10 nm) in the same solution for 2 hours. Finally, the samples were washed in H_2O 3x3 min and contrasted with 2% uranil acetate.

Antibodies

The following antibodies were used: Primary antibodies were goat anti-lamin B (Santa Cruz, sc-6216, 1:100); rabbit anti-GFAP (DAKO, Z0334, 1:500); mouse anti-GFAP (Millipore, MAB360, 1:500); rabbit anti-EGFR (Millipore, 06-849, 1:200); rabbit anti-BLBP (Millipore, ABN14, 1:600); mouse anti-ß-catenin (BD Biosciences, 61053, 1:500); rabbit anti-gamma-tubulin (Sigma, T5192, 1:400); rabbit anti-Glast (Abcam, Ab416, 1:200); mouse anti-Nestin (Millipore, N5413, 1:100); rabbit anti-p57 (Sigma, P035, 1:500); mouse anti-5mC (Abcam, AB10805, 1:100); guinea pig anti-LBR (Harald Hermann, DKFC); rabbit anti-HP1 (Santa Cruz, sc-28735, 1:100); rabbit anti-LAP2 (Santa Cruz, sc-28541, 1:100); mouse anti-actin (Millipore, MAB1501, 1:100); rabbit anti-TRF2 (Santa Cruz, sc-9143, 1:100); rabbit anti-H3K9me3 (Abcam, Ab8898, 1:500) and mouse anti-H3lys27me3 (Thermo Fisher, 05-1951, 1:100). For fluorescent immunostaining, secondary antibodies conjugated to Alexa Fluor dyes were used (goat polyclonal, 1:500; Molecular Probes, Eugene, OR). For pre-embedding immunogold staining the appropriate colloidal gold-conjugated secondary antibodies were used (1:50; UltraSmall; Aurion, Wageningen, The Netherlands). For post-embedding immunogold staining the appropriate 10 nm gold-conjugated secondary antibodies were used (1:50, G-7402, Sigma).

Titrated thymidine autoradiography cell counting

A cell was considered labeled if sic or more silver grains overlaid the nucleus and the same cell was labeled in three or more consecutive semithin sections. For the adult proliferation studies, we analyzed 204 ^{3}H-Thy labeled cells, 30 of which were type B cells with round nucleus. Two months after ^{3}H-Thy, the number of labeled cells was rare. Among more than 8,000 V-SVZ nuclei, only 20 ^{3}H-Thy labeled cells were found. All of these cells were serially reconstructed. For embryonic ^{3}H-Thy birth-dating assays, 25 P0 and 37 P21 ^{3}H-Thy-labeled-cells were studied. However, to confirm the presence or absence of ELCS, we only used for the study those cells which could be completely reconstructed.

***In vitro* assays**

For neurosphere cultures, we dissected the V-SVZ of P60 mice as previously described (Gritti et al., 1999). After digestion with papain, cells were dissociated and seeded in a control medium (DMEM/F12, 2 mm L-glutamine, 0.6%, glucose, 9.6 mg/mL putrescine, 6.3 ng/mL progesterone, 5.2 ng/mL sodium selenite, 0.025 mg/mL insulin, 0.1 mg/mL, transferrin, 2 mg/mL heparin and antibiotic/antimycotic) supplemented with epidermal growth factor (human recombinant EGF, 20 ng/mL: Invitrogen Life Technologies, Carlsbad, CA, USA) and basic fibroblast growth factor (human recombinant FGF, 10 ng/mL; Sigma Aldrich). Stem cells were maintained in vitro at 37 ºC in a humidified 5% CO_2 atmosphere for all the experiments performed. We fixed neurosphere cells with

glutaraldehyde 3% (EMS) at passage one and passage four for TEM analysis. We studied the nuclear morphology of 1000 neurosphere cells (from 10 neurospheres) in semithin and ultrathin sections.

To determine if ELCS could be induced by retinoic acid, we added complete medium with 2, 5 and 10 μM retinoic acid (Sigma, R-2625) to passage 1 neurospheres. After 7 days, we fixed the neurospheres and studied them by TEM. In all experiments, HL60 myeloid leukemia cell line was used as a positive control for ELCS induction by retinoic acid. Different DMSO concentrations (2, 5 and 10 μM) were used as a negative control of the ELCS induction in neurosphere and HL60 cultures.

Mouse V-SVZ monolayer cultures were carried out as previously described (Park et al., 2014). P7-8 mice V-SVZ were micro-dissected and dissociated with 0.25% trypsin with EDTA. Cells were plated at ~30,000 cells/cm^2 in 6-well plates (Corning) in proliferation medium (DMEM/F12, 5% FCS, 20 ng/mL EGF, 20 ng/mL bFGF, 35 μg/mL bovine pituitary extract (media and N2 are from Invitrogen; growth factors are from Peprotech; FCS is from Hyclone). Non-attached cells were collected after 1 day and re-plated into 6-well plates. After ~7 days, the cells were confluent and these were routinely passaged 1:2 with 0.25% trypsin. Culture differentiation was induced by removing EGF and FGF from media.

For ELCS analysis in monolayer cultures, we fixed cultured cells with 3% glutaraldehyde at passage 1 and studied 1,000 monolayer cultured cells under semithin and ultrathin sections. To study ELCS presence in differentiated monolayer cultured cells, we fixed cells after removing EGF and FGF. Additionally, we studied passage 1 cells without adding any grow factors and using Neurobasal B27.

All *in vitro* results were obtained from 3 independent replicates.

Supplemental References

Gritti, A., Frölichsthal-Schoeller, P., Galli, R., Parati, E.A., Cova, L., Pagano, S.F., Bjornson, C.R., Vescovi, A.L., 1999. Epidermal and fibroblast growth factors behave as mitogenic regulators for a single multipotent stem cell-like population from the subventricular region of the adult mouse forebrain. Journal of Neuroscience 19, 3287–3297.

Mirzadeh, Z., Merkle, F.T., Soriano-Navarro, M., Garcia-Verdugo, J.-M., Alvarez-Buylla, A., 2008. Neural Stem Cells Confer Unique Pinwheel Architecture to the Ventricular Surface in Neurogenic Regions of the Adult Brain. Stem Cell 3, 265–278. doi:10.1016/j.stem.2008.07.004

Park, D.H., Hong, S.J., Salinas, R.D., Liu, S.J., Sun, S.W., Sgualdino, J., Testa, G., Matzuk, M.M., Iwamori, N., Lim, D.A., 2014. Activation of Neuronal Gene Expressionby the JMJD3 Demethylase Is Requiredfor Postnatal and Adult Brain Neurogenesis. CellReports 1–10. doi:10.1016/j.celrep.2014.07.060